



This is to certify that the
thesis entitled

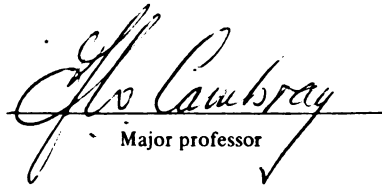
A Geophysical and Geological Study of the Basement Complex
Along the Peshekee River, Marquette County, Northern Michigan

presented by

David C. Shanabrook

has been accepted towards fulfillment
of the requirements for

Masters degree in Geology


Major professor

Date 5/16/78

© Copyright by
DAVID CLARK SHANABROOK
1978

A GEOPHYSICAL AND GEOLOGICAL STUDY OF
THE BASEMENT COMPLEX ALONG THE PESHEKEE RIVER,
MARQUETTE COUNTY, NORTHERN MICHIGAN

By

David Clark Shanabrook

AN ABSTRACT OF A THESIS

Submitted to
Michigan State University
in partial fulfillment of the requirements
for the degree of

MASTER OF SCIENCE

Department of Geology

1978

G113736

ABSTRACT

A GEOPHYSICAL AND GEOLOGICAL STUDY
OF THE BASEMENT COMPLEX ALONG THE
PESHEKEE RIVER, MARQUETTE COUNTY,
NORTHERN MICHIGAN

By

David Clark Shanabrook

The purpose of this study was to test a new computer-aided geophysical interpretation method developed by the author. After testing, it seems clear that this method, which takes into account both the induced and remanent components of the observed magnetic field, can be used to project units from areas of known geology into poorly known or unexplored areas. This method can also be used to determine a body's remanent magnetic vector with a fair degree of accuracy. This vector can then be used to help establish the body's absolute age in many cases.

Geologic and paleomagnetic studies conducted in conjunction with the test of the new method led to these additional conclusions:

1. The Y-age diabase in the area yields a paleopole at 148°W longitude, 42.5°N latitude.
2. The main compressive stress of the Penokean Orogeny in this area, as determined from the foliation and shearing patterns of metadiabase dikes, acted along a northeast-southwest line.
3. An amphibolite, believed to be correlative with part of the Mona Schist, outcrops in a series of east-west trending folds.

ACKNOWLEDGMENTS

The author wishes to express appreciation to Dr. F. W. Cambray, Chairman of the Department of Geology, Michigan State University, under whose guidance this study was undertaken, for his suggestions and assistance.

Thanks are also extended to Dr. James Trow and Dr. John Wilband, other members of the guidance committee, for their suggestions and critical examination of the manuscript.

The author also wishes to thank Dr. Robert VanderVoo of the University of Michigan for use of his paleomagnetic laboratory and equipment.

Gratitude is expressed to William Ciolek, Mark Fortuna, Mark Locher, Michael Ritter, and many others who gave generously of their time and skill during the course of this study.

Sincerest appreciation is also expressed to my parents, Mr. and Mrs. L. D. Shanabrook, for their encouragement and help during this study as well as the rest of my educational career.

TABLE OF CONTENTS

	Page
LIST OF TABLES	iv
LIST OF FIGURES	v
INTRODUCTION	1
General Geology and Geophysics	4
Location and Topography	5
Field and Laboratory Methods	8
GEOLOGY	9
Mineralogy and Description of Units	9
Y-age (Keweenawan) Diabase	9
X-age (Proterozoic) Metadiabase	12
W-age (Archean) Amphibolite	15
W-age (Archean) Gneisses	17
Structure	19
GEOPHYSICS	29
Interpretation	29
Paleomagnetism	37
DISCUSSION AND CONCLUSIONS	48
APPENDIX A	53
APPENDIX B	73
APPENDIX C	81
BIBLIOGRAPHY	83

LIST OF TABLES

Table	Page
1. Average magnetic susceptibility of the various rock units studied in cgs units	32
2. Comparison of paleomagnetic data	34
3. Data used in determining Y-age paleopole	44
4. A complete listing of SHALOCI	54
5. Yellow Dog Plains Peridotite - observed magnetic field values with the calculated field values (listed below observed value), and residuals	77
6. Yellow Dog Plains Peridotite - calculated remanent magnetic field values and unexplained residuals	79

LIST OF FIGURES

Figure	Page
1. Chronology and sequence of events	2
2. Geology from earlier studies	3
3. Contoured ground magnetic data	6
4. Location of the study area	7
5. Outcrops of Y-age diabase	10
6. Example of the en echelon pattern of the Y-age diabase	11
7. Outcrops of X-age metadiabase	13
8. Outcrops of Mona Schist, and tonalitic and granitic gneisses	16
9. Foliations of the gneiss and banding of the Mona Schist	20
9a. Facepoles to the foliation of the gneiss	21
9b. Facepoles to the banding of the Mona Schist	22
10. Facepoles to foliation and banding	23
11. Structural cross-section through the study area	25
12. Foliation and shearing of X-age dikes	26
13. Model to explain the foliation and sheared margins of the metadiabase dikes	27
14. Data processing procedures	30
15. Traces of linear lows from the second derivative map	31
16. Contour map of the vertical magnetic field due to the Y-age diabase	35
17. Residual map	36

Figure	Page
18. AC-demagnetization curve for Y-age diabase samples	38
19. A typical AC-demagnetization with peak AC field in oersteds given	39
20a. Y-age diabase, pre-AC cleaning	40
20b. Y-age diabase cleaned in AC field of 100 oe	41
21a. Y-age diabase pre-thermal cleaning	42
21b. Y-age diabase thermally cleaned	43
22. Apparent polar wandering track from Irving and McGlynn	46
23. NRM directions of X-age metadiabase	47
24. Geologic map of the study area	49
25. Coordinate system used in SHALOCI	60
26. Magnetic declination and inclination	64
27. Remanent vector inclination and declination	64
28. Order of data input for card series 8	71
29. Example of ring-averaging	71
30. Anomaly separation for SHIFT	71
31. Data extension pattern of SHIFT	72
32. Observed total magnetic field values, Yellow Dog Plains Peridotite	74
33. Natural remanent magnetic field, Yellow Dog Plains Peridotite	75
34. Model of the Yellow Dog Plains Peridotite	76
35. Residual (model-observed) for the Yellow Dog Plains Peridotite	80

INTRODUCTION

The purpose of this study is to test a new method of magnetic interpretation developed by the author by comparing the geology actually observed in the field with geological models derived from the data using the new interpretational techniques.

The new method presented here uses a computer program that takes into account both the remanent and the induced parts of the observed magnetic anomaly to produce models of an area from the geophysical data. It does so by extending units from areas of known geology into the areas where the geology is not known. Since this computer program does take remanent magnetic vectors into account, it can also be used to determine a body's remanent vector by calculating the induced field and subtracting it from the observed field. In many cases, this remanent vector can then be used to help date the geologic unit it was extracted from.

A 15-square kilometer area along the Peshekee River north of Lake Michigamme, Marquette County, Michigan was selected as the study site. The geology of the area consists of a tonalitic gneiss overlain by an amphibolite, both of which are intruded by a later granitic gneiss. All of these units are cut by mafic bodies of Precambrian X and Y-age (Figure 1). Due to the complex picture of the geology advanced by earlier studies (Bodwell, 1972; see Figure 2) and the poor rock exposure in most of this area, the western and northern parts of the area were remapped by the author. These mapped regions then served as reference

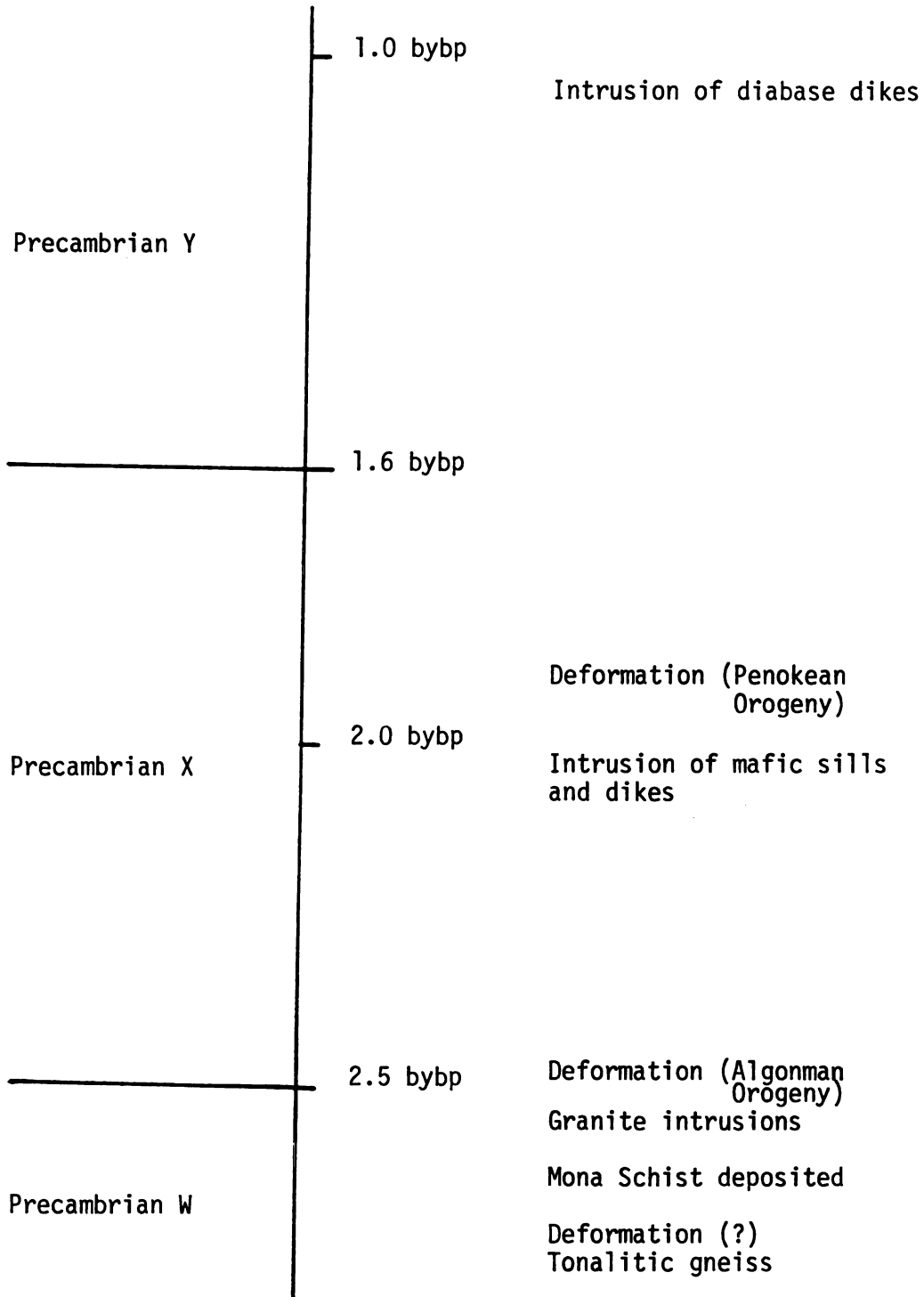


Figure 1. Chronology and sequence of events (time scale from Cannon and Gair, 1973; Algonman and Penokean Orogenies as defined by King, 1969, and Goldich et al., 1961).

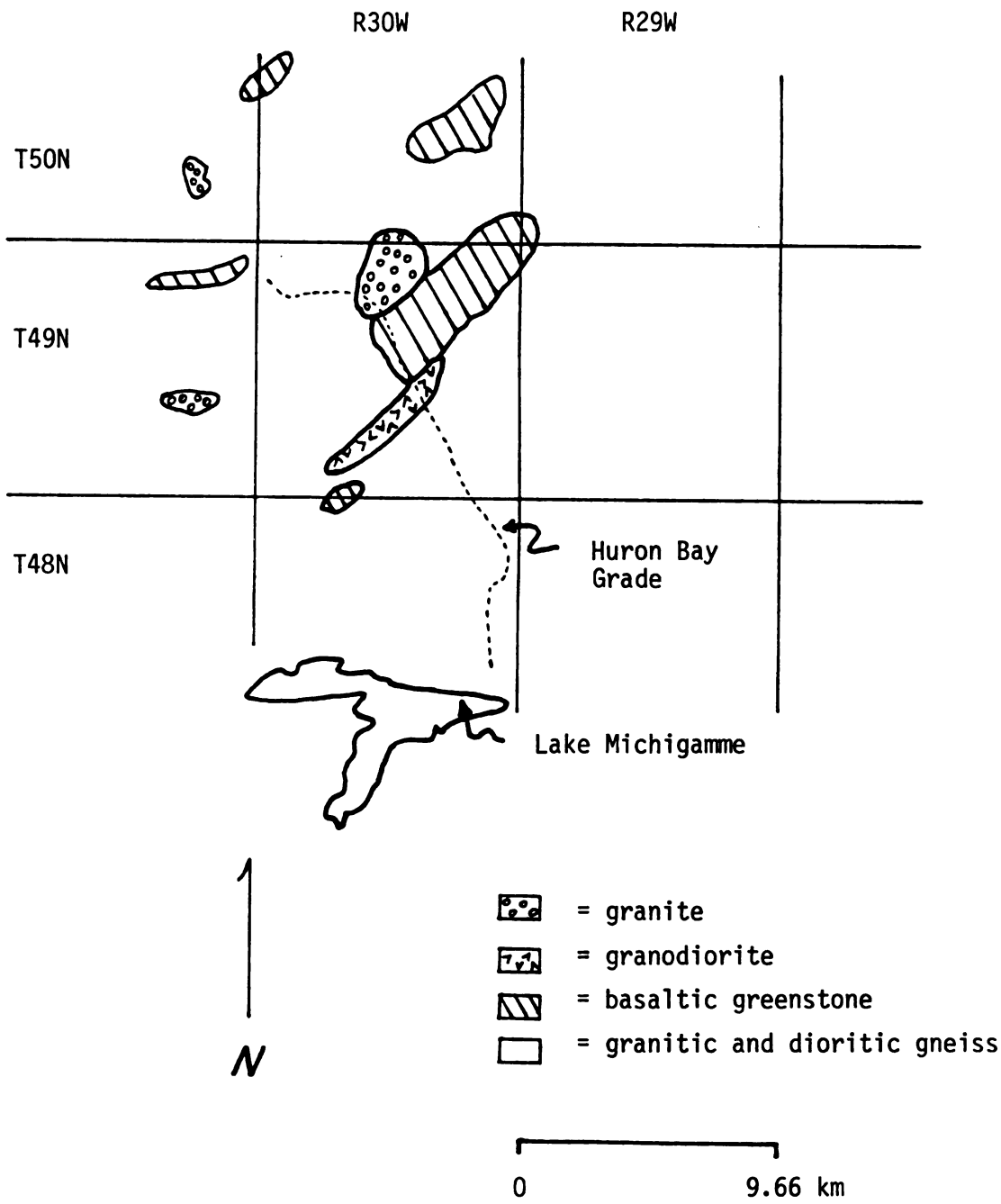


Figure 2. Geology from earlier studies (after Bodwell, 1972).

areas for the interpretation of the ground magnetic data.

The new method of magnetic interpretation outlined here could become a powerful tool used to complement field mapping work in igneous or metamorphic terranes, and with some slight modifications, it could be used in areas of more substantial sedimentary cover.

General Geology and Geophysics

The predominant geologic units of the study area are a well foliated tonalitic gneiss and a well banded amphibolite. The amphibolite appears to unconformably overlie the gneiss in some areas but the intense deformation associated with the Algoman Orogeny (2.5 bybp) has made their original relationship unclear. The amphibolite is intruded by another, slightly deformed granite that penetrates the amphibolite along its banding in most areas. All three of these units are cut by Precambrian X-age metadiabase dikes which vary in orientation and which contain numerous xenoliths of the wall rock in many locations. These metadiabase dikes generally have sheared margins and internal foliations produced during the Penokean Orogeny (1.90-1.95 bybp). All of the preceding units are cut by Keweenaw (or Y-age) diabase dikes that are extremely fresh and show no signs of any type of deformation. These east-west trending dikes are part of a 100-kilometer long swarm of diabase dikes that stretch from near the Keweenaw Fault to beyond the city of Marquette (Bodwell, 1972; Case and Gair, 1965; and the U.S. Geological Survey, 1967). This swarm of dikes is believed to have been emplaced around 1.1 billion years ago during an episode of continental rifting (Chase and Gilmer, 1973).

The ground magnetics of the study area are very flat except for

the intense lows associated with the Y-age diabase dikes and the moderate highs associated with the X-age metadiabase bodies (Figure 3). The lows associated with the Y-age diabase dikes are due to the fact that the dikes are reversely polarized. That is to say, these dikes have an effective magnetic vector that substantially decreases the earth's magnetic field in their vicinity. The metadiabase dikes, on the other hand, have effective magnetic vectors that are oriented so as to increase the earth's magnetic field. The magnetic anomalies produced by these strongly magnetized rocks mask any variations in the magnetic field that might be due to the contrast between gneiss and amphibolite, both of which are only weakly magnetic.

Location and Topography

The study area is located about 55 kilometers west-northwest of the city of Marquette, Michigan and 15 kilometers north of Lake Michigamme along the Huron Bay Grade (Figure 4) in the northwest corner of Marquette County. The area covers about 15 square kilometers in sections 9, 10, 11, 13, 14, 15, 21, 22, and 23 of T49N, R30W of the Champion quadrangle and is easily accessible along the Huron Bay Grade.

The area consists of a series of high ridges separated by sharp-sided valleys, many of which contain bogs, streams, or lakes. The ridges are composed of gneiss, amphibolite, or metadiabase and rise 15 to 160 meters above the surrounding terrain. The valleys generally trend east-west and are believed to be underlain by Y-age diabase dikes covered by Pleistocene outwash and till. The region is poorly drained and most of the low-lying areas are covered by cedar swamps and dense

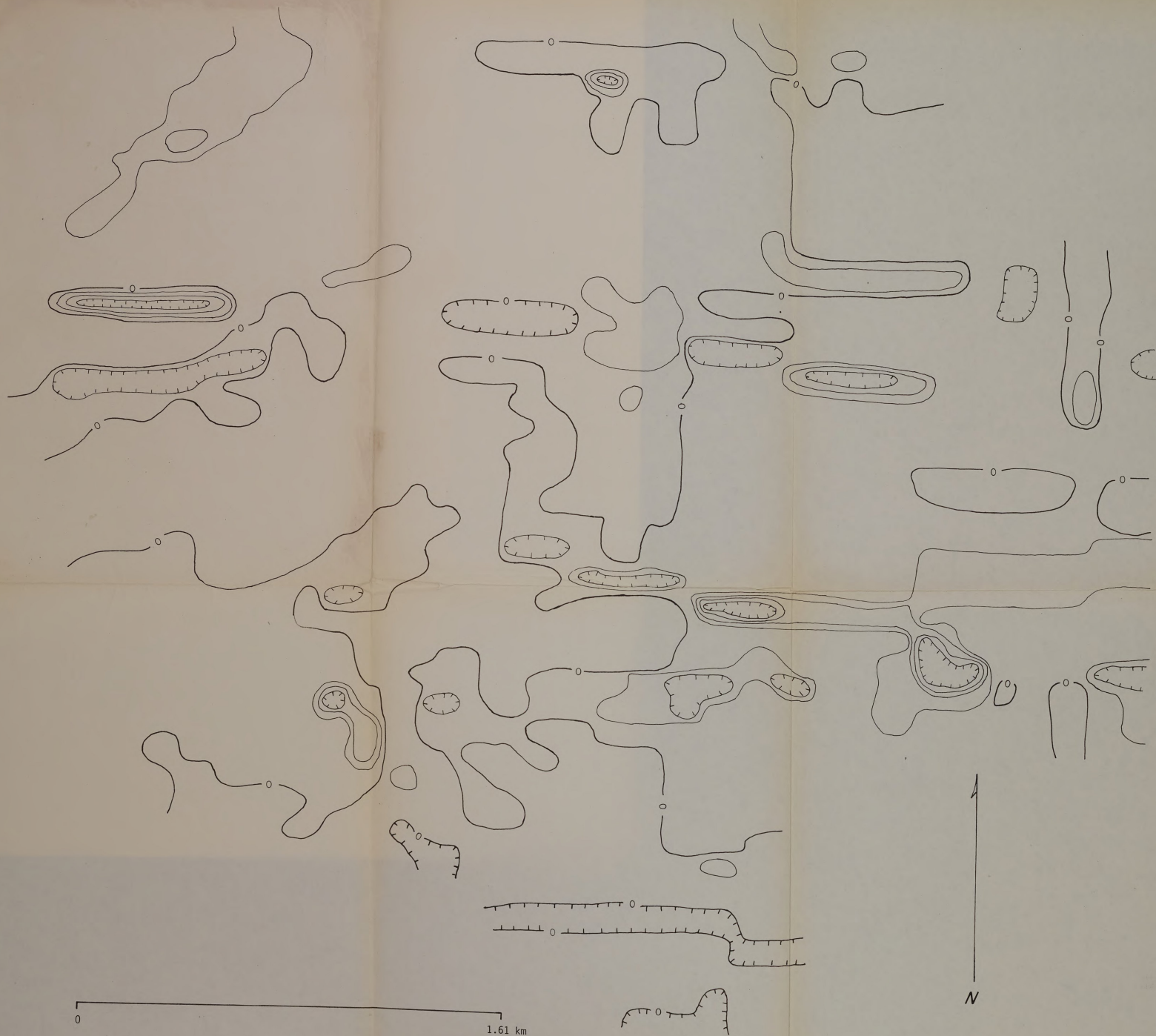


Figure 3. Contoured ground magnetic data (C.I.= 300 gammas).



Figure 4. Location of the study area.

thickets of alder bushes. The higher ridges are somewhat better drained but are generally covered with thick stands of deciduous trees with an underbrush consisting of mosses and grasses.

Field and Laboratory Methods

The western half of the area was geologically mapped along traverses designed to intersect the maximum amount of outcrop possible. Directions and distances along the traverses were established by pace and Brunton compass. North-south ground magnetic survey lines with station spacings of 30 meters were also laid out using the pace and compass method. Magnetic readings were later made along these lines as well as all available roads with a Sintrex Fluxgate Magnetometer. These field readings were corrected for elevation to the nearest three meters and drift before being used in the interpretation process. Since these two corrections never changed the observed value by more than 100 gammas, it is felt that readings more than 200 gammas above or below neighboring observations are significant.

Oriented blocks of each of the rock types were collected in the field from the most accessible outcrops. Cores with an inner diameter of 2.54 centimeters were then taken from each sample and analyzed on a Minnetech Magnetic Susceptibility Bridge, model MS-3. The cores from the Y-age diabase dikes and some of the X-age metadiabases were later used for paleomagnetic work by the author at the University of Michigan. Standard AC and thermal demagnetization procedures were followed at all times during this work. The procedures used in the computer-aided interpretation of the ground magnetics are explained in detail in Appendix B.

GEOLOGY

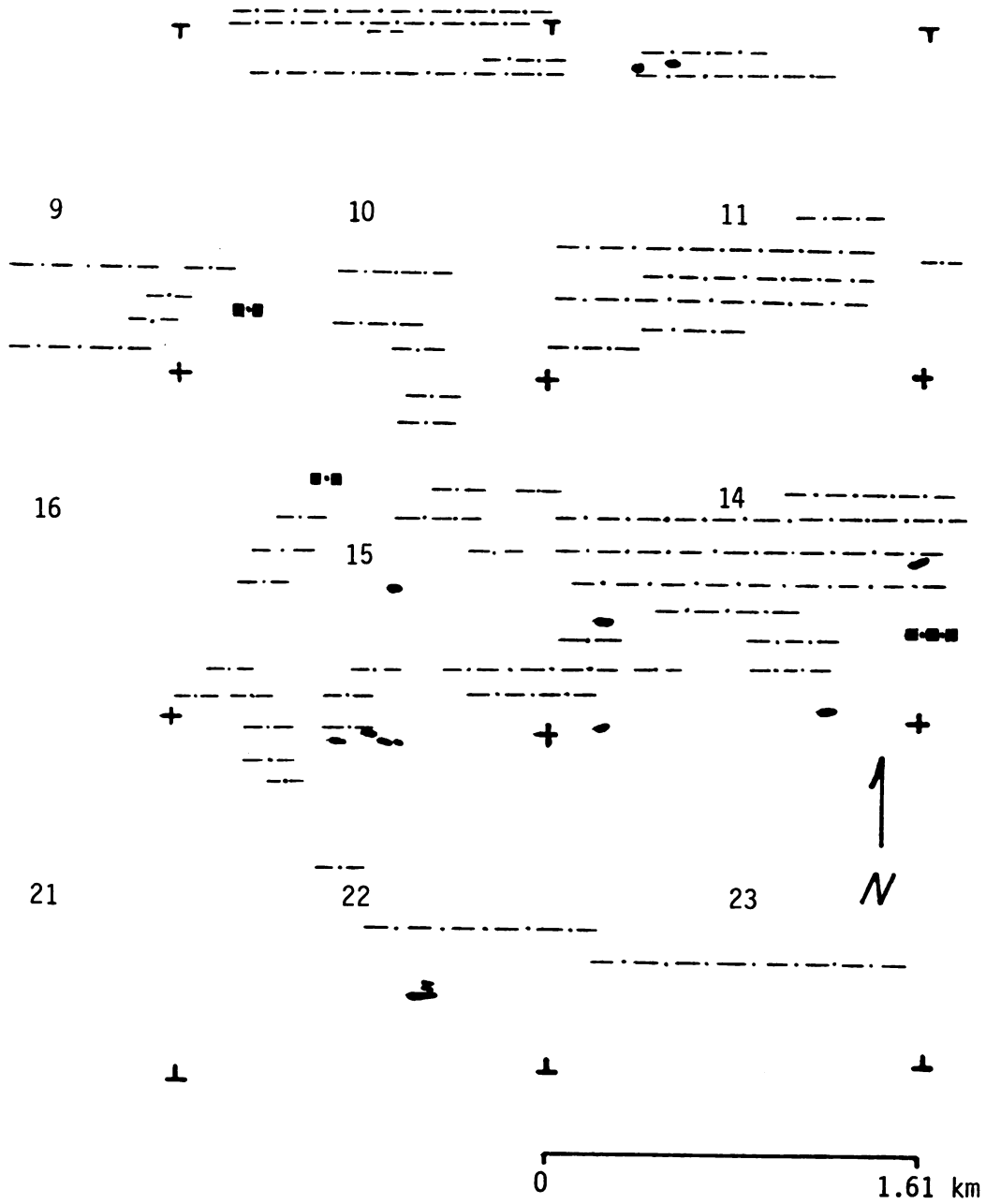
Mineralogy and Description of Units

Specimens of each of the rock units were collected in the field and then examined petrographically. All determinations of composition were made optically.

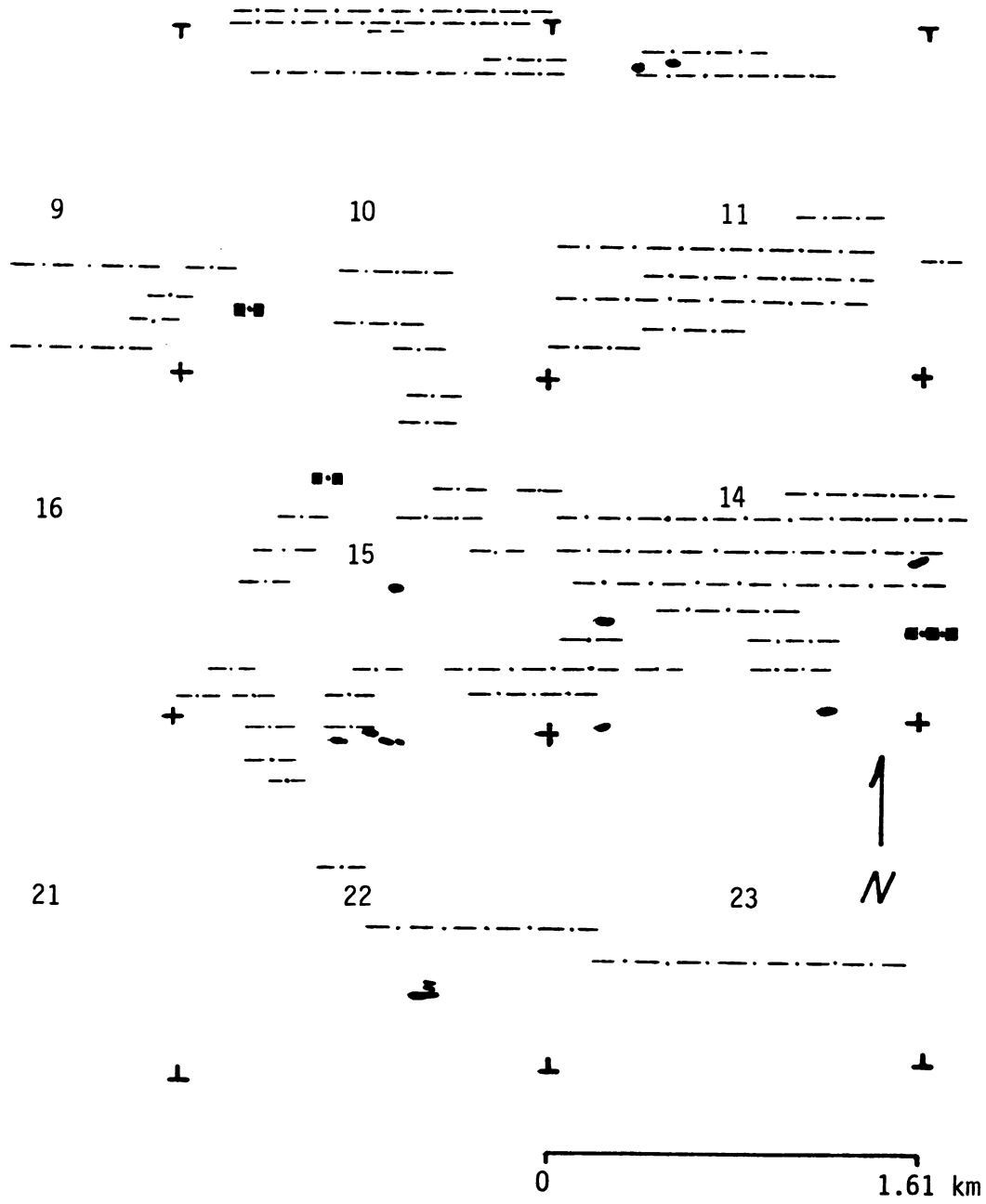
(1) Y-age (Keweenaw) Diabase

This diabase occurs in east-west trending dikes that outcrop several places in the survey area (Figure 5). The dikes range between 2 and 13 meters in width and none exceed 100 meters in length. The dikes tend to be arranged en echelon in most areas. A good example of this can be seen in the NW, NW, NE of section 22 (Figure 6). The diabase outcrops tend to be low, rounded masses, gray-blue to black in color, which are heavily jointed.

The composition of the diabase, using visual estimates of mineral content from thin section work, is estimated to be 50 to 60 percent plagioclase feldspar (An_{54-61} , from the Michel-Lèvy method), 30 to 40 percent diopsidic augite, 5 to 10 percent opaque minerals, and less than 10 percent hornblende and biotite. In coarser grained samples, up to 15 percent of the rock may be composed of large olivine grains or serpentine pseudomorphic after olivine. Over 95 percent of the opaque mineral content in the diabase dikes is magnetite. The magnetite either occurs as fine grains disseminated throughout the rock or as clusters of irregularly shaped grains near olivine or serpentine



or = outcrop of Y-age diabase + = section corners
 - - - - - = trace of magnetic low



or = outcrop of Y-age diabase + = section corners
 = trace of magnetic low

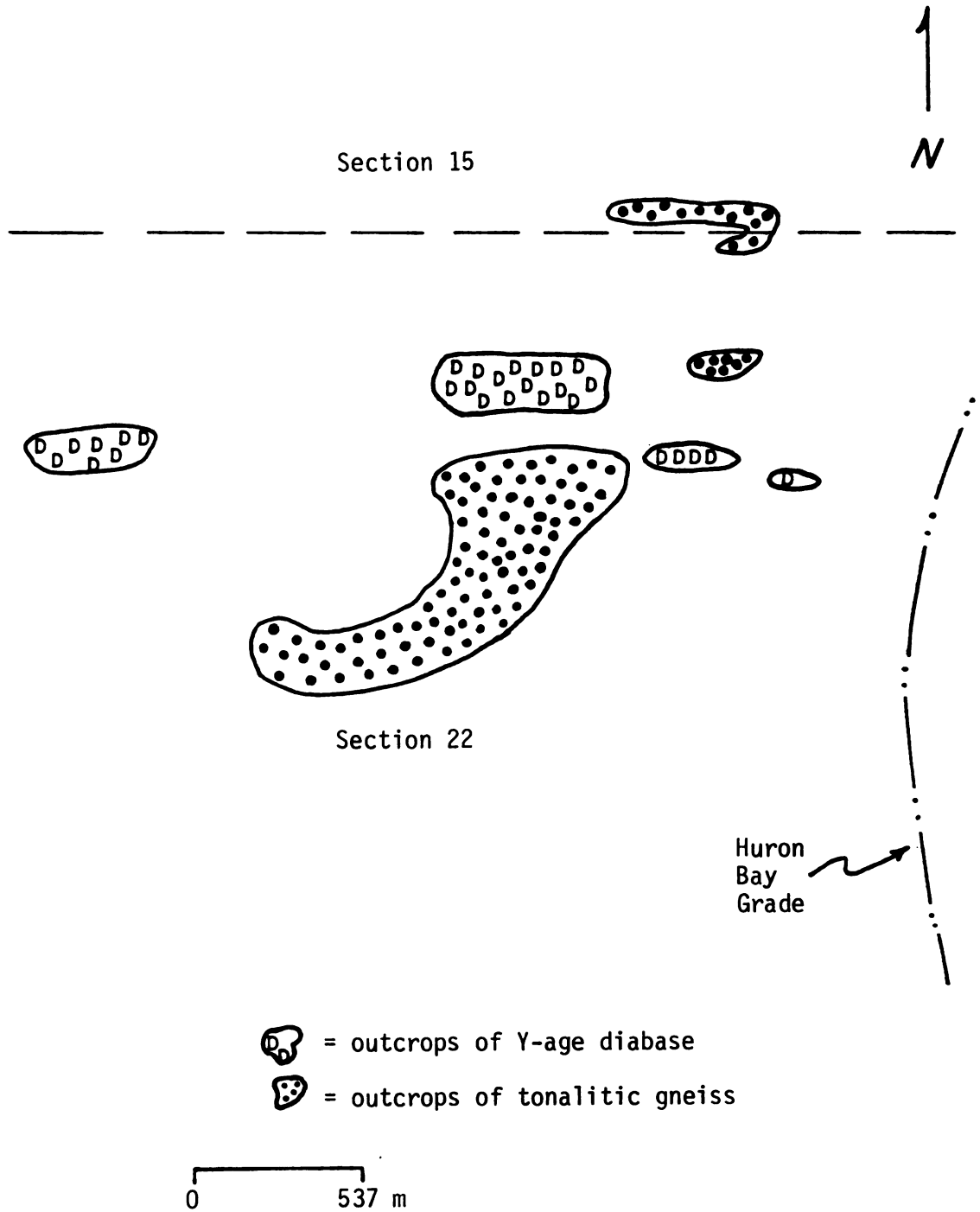


Figure 6. Example of the en échelon pattern of the Y-age diabase.

grains. Some of the magnetite has been altered to hematite. About 4 percent of the opaque grains are euhedral pyrite crystals that occur randomly throughout the rock. The remaining opaque grains are bornite crystals that occur near some of the magnetite clusters.

All the samples that were examined but one had biotite and hornblende grains present. These minerals may be alteration minerals that formed from the original pyroxenes during the cooling and dewatering of the diabase. Despite this deuteric alteration, the diabase samples still display a fresh, ophitic texture of pyroxenes and distinctly twinned laths of plagioclase, many of which are normally zoned.

The Keweenawan diabases are the youngest rocks in the area and have been observed to cut every unit but the X-age metadiabases in the field. However, they are believed to post-date these metadiabases based on their fresh textures, their lack of internal foliations and sheared margins, their mineralogy, and the clear difference in remanent magnetism between the diabases and the metadiabases (Figures 20b, 21b, and 23).

(2) X-age (Proterozoic) Metadiabase

The metadiabase dikes occur as irregularly shaped bodies with variable orientations that outcrop throughout the study area (Figure 7). The bodies range in size and shape from 1 meter-wide vertical sheets that can only be traced for 6 meters along strike to irregular masses that are up to 30 meters wide and 200 meters long. The dike-like bodies almost all have internal foliations and sheared margins while the larger, more irregularly shaped ones do not have these features. The metadiabase outcrops vary in color from pale tan or light

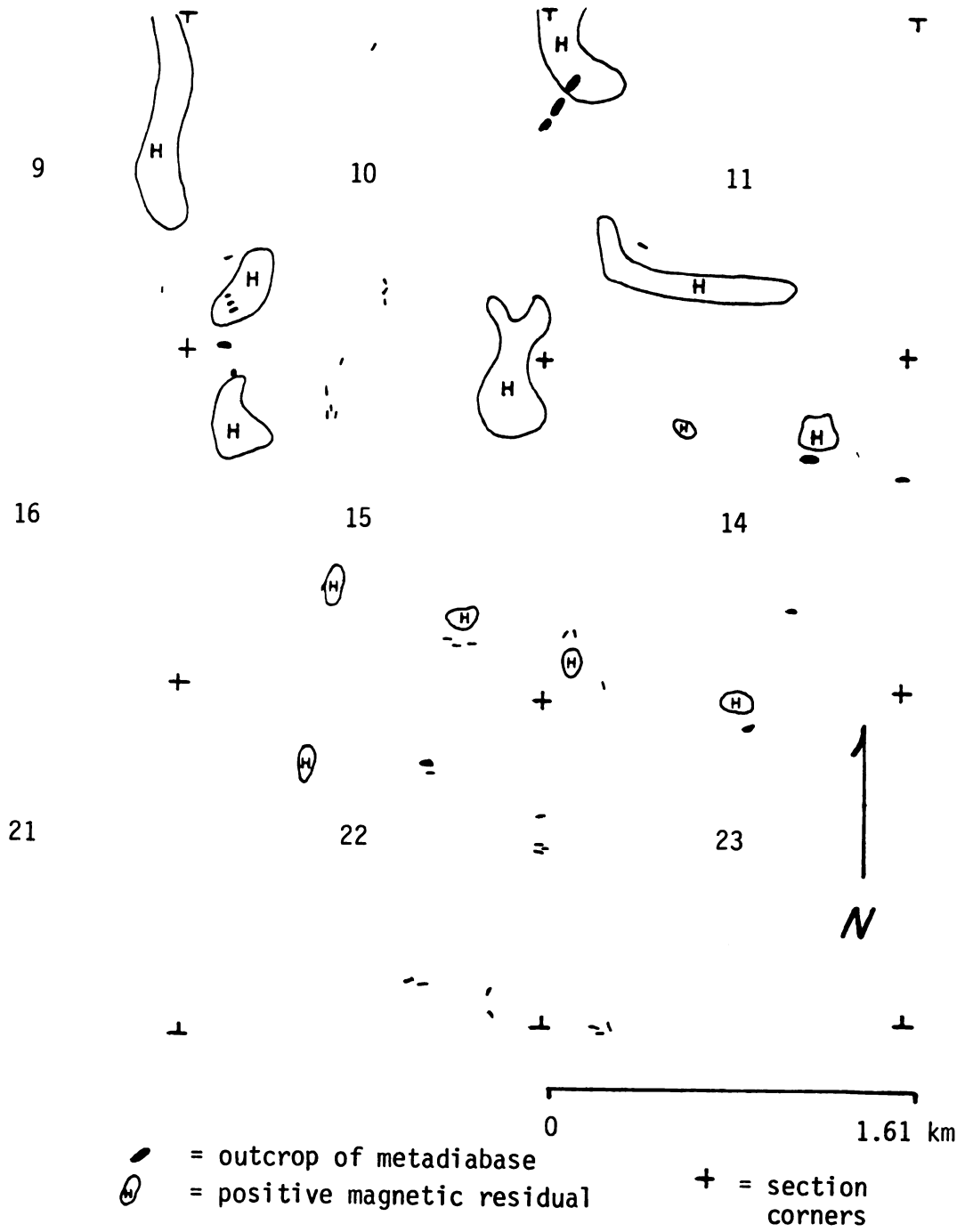


Figure 7. Outcrops of X-age metadiabase.

gray-green to a dark blue-gray. Many of them form high, steep sided hills, and they are generally poorly jointed.

The metadiabases are mineralogically and texturally highly variable. In some, there are relics of large pyroxenes and zoned plagioclases suggestive of a primary gabbroic texture while in others, in the sheared margins, the original texture has been entirely replaced by aligned biotite, chlorite, and plagioclase grains. The most common minerals are plagioclase, amphiboles of the actinolite-tremolite series, epidote, chlorite, pyrite, and magnetite. Plagioclase with cloudy centers consisting of epidote and chlorite with clear albitic rims is common in these rocks while some amphibole and chlorite are pseudomorphic after the pyroxenes they replaced. Pyroxene, biotite, sphene, and calcite are also found in small amounts in some of the samples. Most of the magnetite in these metadiabases occurs in skeletal masses in relics of pyroxene or hornblende while the pyrite occurs as euhedral grains of various sizes disseminated throughout the rock.

The Proterozoic metadiabases and metagabbros intrude every unit in the area except the Y-age diabase dikes. These Precambrian X-age mafic intrusives are of at least two distinct ages since one of the irregularly shaped metagabbros is cut by two metadiabase dikes. The common occurrence of albite, calcite, and epidote in these rocks indicates that they have been metamorphosed to at least the upper Greenschist facies. This metamorphism is thought to have occurred during the Penokean Orogeny (1.9-1.95 bybp). This orogeny is also thought to have caused the foliation and shearing observed in the more dike-like bodies.

(3) W-age (Archean) Amphibolite

The amphibolite outcrops in the northeastern and eastern parts of the survey area (Figure 8). The outcrops range in size from low ridges that are 2 meters high, 10 meters wide, and 30 meters long to cliff-faces that are 25 meters tall and well over 150 meters long. The amphibolite weathers to a light to medium green color and shows a distinct 5 to 7 centimeter banding. The amphibolite is very poorly jointed although it does contain a number of small folds and a few reverse faults with displacements of less than 1 centimeter.

The amphibolite tends to be fairly coarse grained, although there is considerable variation, and the amphiboles in the rock are generally well aligned forming a penetrative lineation, although some samples do preserve a number of relict pyroxenes and a good deal of original igneous texture. The main constituents of the amphibolite in decreasing order of importance are hornblende, quartz, chlorite, epidote, and plagioclase. Calcite, sphene, hematite, pyrite, biotite, and magnetite are also present in trace amounts in some of the samples. Several of the rock samples contain large, relict pyroxenes that seem to be original igneous grains rather than metamorphic minerals. These relict pyroxenes can comprise up to 15 percent of some of the rock samples. The hornblende grains which make up 65 to 70 percent of all of the samples are also very large, and they usually display very euhedral shapes and have sharp grain boundaries. The quartz grains, on the other hand, which compose 15 to 20 percent of the amphibolite, have only moderate sizes and display well developed strain lamellae.

On the basis of its distinctive banding, intermediate chemical composition, and its stratigraphic position, the Archean amphibolite

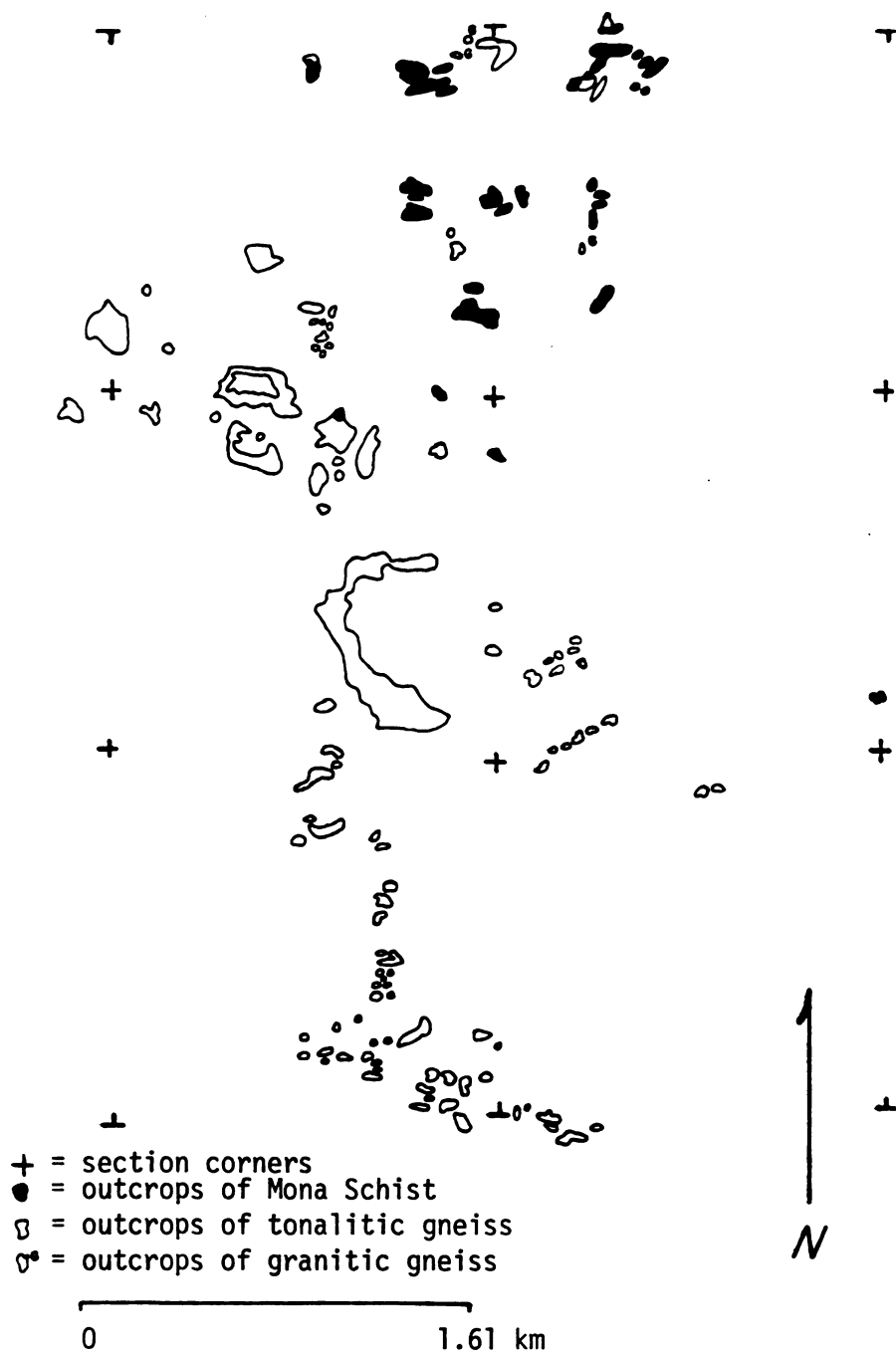


Figure 8. Outcrops of Mona Schist, and tonalitic and granitic gneisses.

in this area is thought by the author to be part of the Lighthouse Point Member of the Mona Schist which is also finely banded and is of a similar chemical nature. In the study area, the amphibolite rests unconformably on a tonalitic gneiss, but like the Mona, it is intruded from below by a gneiss of granitic composition. The granitic gneiss has penetrated the amphibolite along its well developed banding in many areas, often wedging large blocks of the amphibolite out of their original positions into 1 to 2 meter wide dikes of granitic material.

The W-age amphibolite in this area (hereafter referred to as the Mona Schist) is thought to have been deformed and metamorphosed during the Algoman Orogeny (2.5 bybp). It is possible that the Mona's distinctive banding was developed during this orogeny but it seems more reasonable to suppose that it represents an original layering in the rock. This layering may be igneous or sedimentary in origin but it was impossible to resolve this problem with the data available. It seems that the later Penokean Orogeny had little effect on this unit although it would be difficult to tell where the metamorphic effects of one ended and the other began.

(4) W-age (Archean) Gneisses

There are two gneisses exposed in the survey area: one of tonalitic composition that outcrops over most of the area studied and a second one of granitic composition that intrudes the Mona in many areas and is exposed in the NE, NE of section 10 (Figure 8). The tonalitic gneiss is well foliated with distinct bands that average about 15 mm in width, and is generally grayish-white in color. The granitic gneiss on the other hand displays no noticeable banding, and it has a lineation of

plagioclase and strained quartz grains that can only be clearly seen in thin section. The granitic gneiss is usually pink or pale red in color and lacks the sheared brecciated zones that are fairly common in the tonalitic gneiss. The gneisses tend to be exposed as flat patches along the slopes of hills or as cliff faces on the flanks of ridges. The outcrops vary in size from a few square meters to over a quarter of a square kilometer, and almost all of them are covered with gray moss and lichens.

The tonalitic gneiss is medium grained and is composed primarily of plagioclase (An_{27-29}), quartz, and potassium feldspar. Biotite, chlorite, and hornblende comprise 3 to 5 percent of all of the samples, and a few grains of epidote, microcline, sphene, and pyrite are present in some of the samples. The plagioclase grains which compose 60 to 65 percent of the gneiss all have strained twin lamellae. The quartz grains which make up 25 to 30 percent of the gneiss also show a response to stress in the form of strain lamellae.

The granitic gneiss is composed of 25 to 35 percent quartz, 30 to 35 percent plagioclase (An_{26-28}), 30 to 35 percent potassium feldspar, and less than 5 percent biotite and magnetite. None of the plagioclases in this gneiss has strained twinning although the quartz does have strain lamellae, and is fractured in some instances.

The tonalitic gneiss is the oldest rock type in the area studied. It would seem probable that it was in a deformed state when the Mona was deposited on top of it since even though they seem to have been deformed into similar patterns by the Algoman Orogeny, there is a small but real difference between the banding of the Mona and this gneiss where the contact can be clearly seen. The granitic gneiss, on the

other hand, seems to have been deformed much less based on the petrologic information. Further, the amphiboles in the xenoliths of Mona Schist that it contains had already been aligned before they were engulfed by the gneiss since the amphiboles' present alignment is not the same as that of the amphiboles in the adjacent mass of Mona. This seems to imply that the granitic gneiss was intruded during the Algomian Orogeny, and hence it is less deformed than both the tonalitic gneiss and the Mona Schist.

To summarize the preceding sections, the oldest unit in the study area is a tonalitic gneiss. The intermediate volcanics of the Mona Schist lie unconformably on this gneiss. The Mona and presumably the older gneiss are intruded by a granitic gneiss. All three of these units are cut by Precambrian X-age metadiabases and metagabbros. These X-age mafic rocks are in turn cut by diabase dikes of lower middle Keweenawan age (see Figure 1).

Structure

The foliations of the gneiss and the banding of the Mona Schist are plotted in Figure 9. It is evident that the foliations in the southern two-thirds of the region trend east-west and dip steeply to the south. In the northern third of the area, the structure becomes somewhat more complex. Here the foliation and banding trends west-north-west and dips to the north. The poles to the foliation of the gneiss and the banding of the Mona are plotted in Figures 9a and 9b. When plotted together on a stereonet, the poles to the banding and foliation tend to fall together in two clusters (Figure 10). This overlap of the facepoles from these two units seems to indicate that

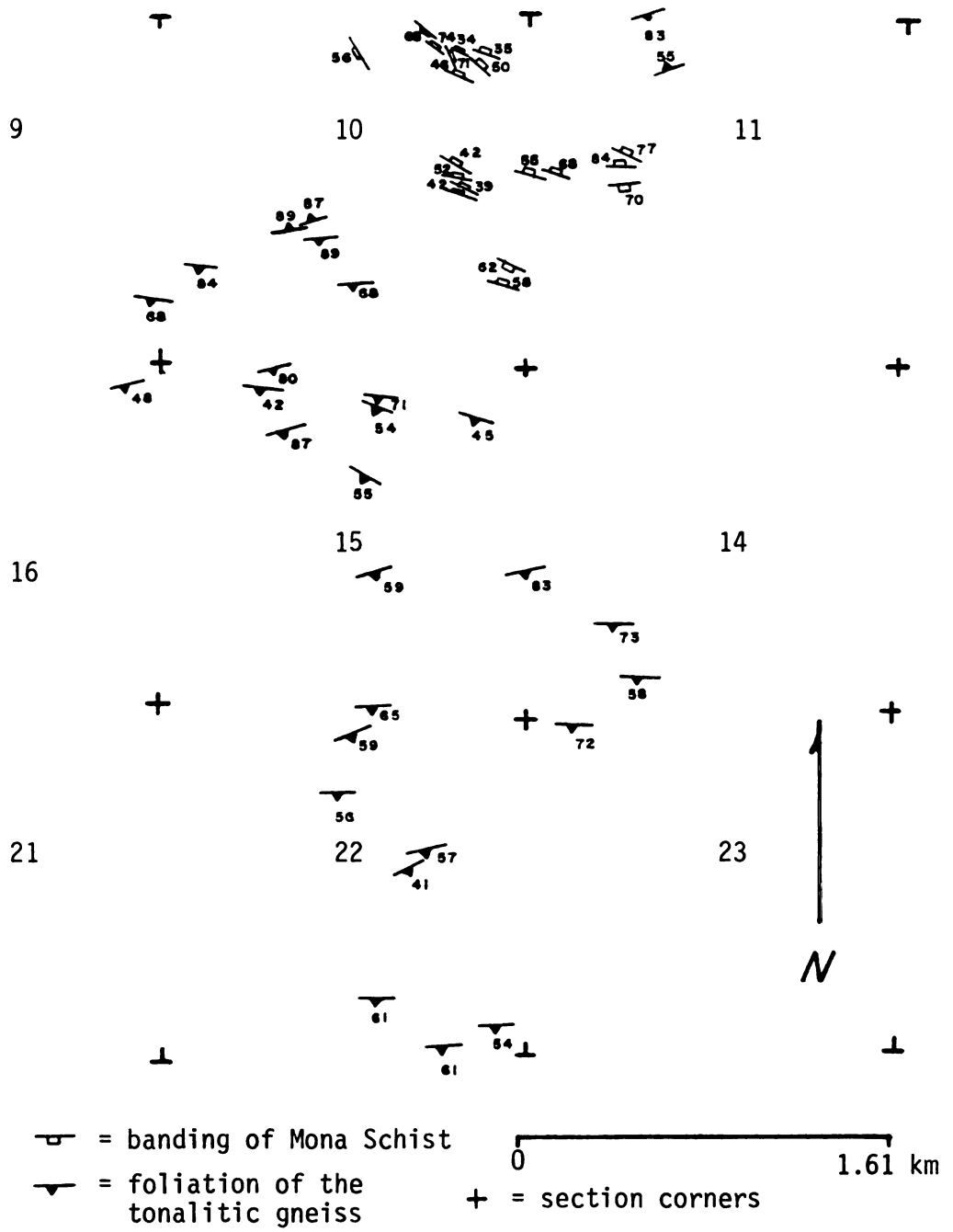


Figure 9. Foliations of the gneiss and banding of the Mona Schist.

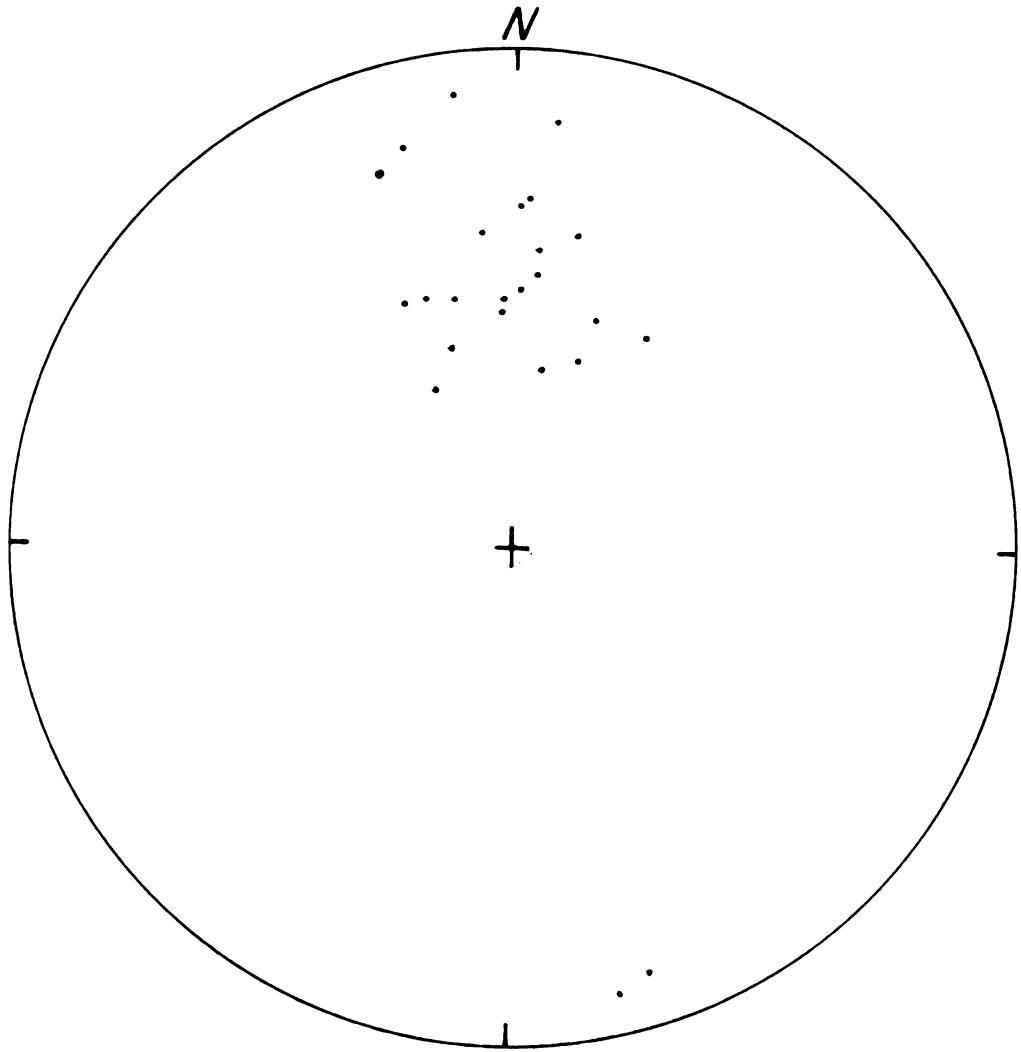


Figure 9a. Facepoles to the foliation of the gneiss.

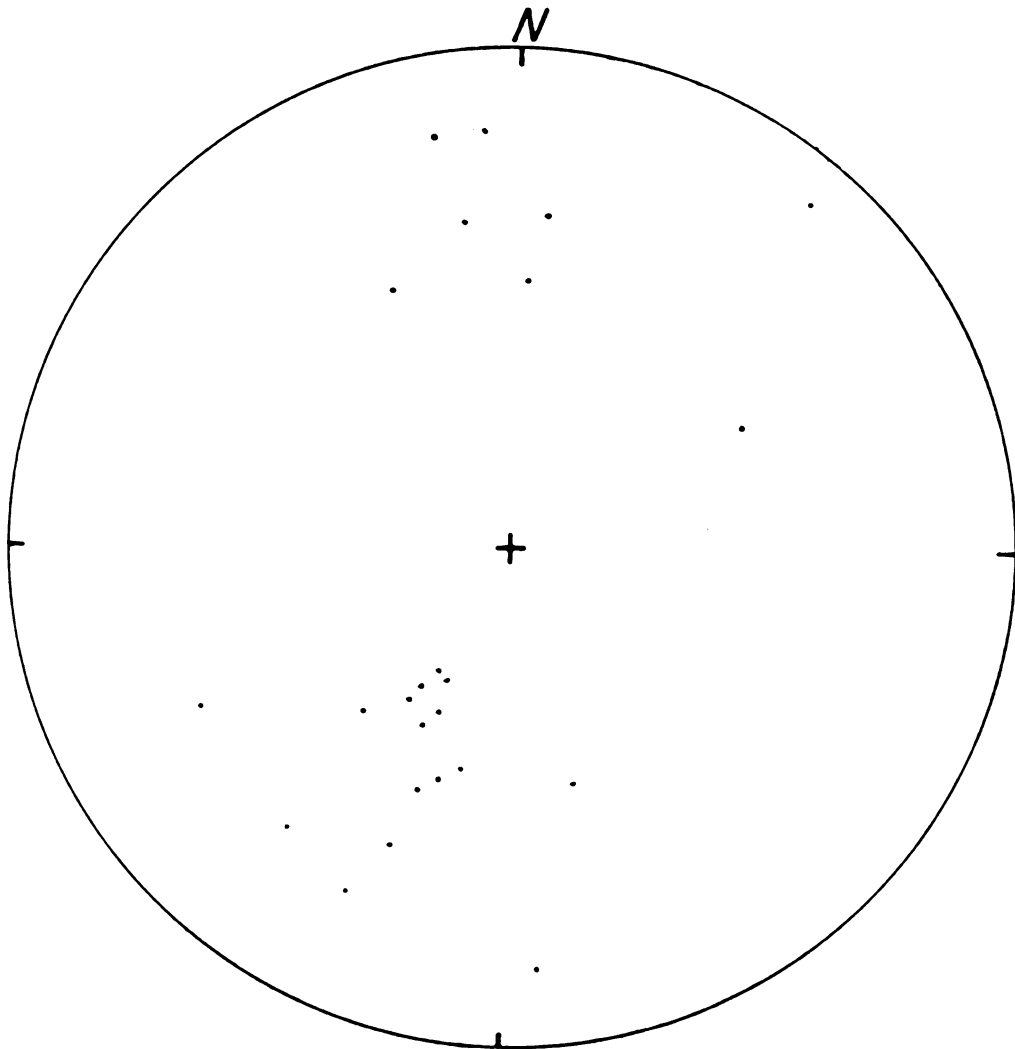
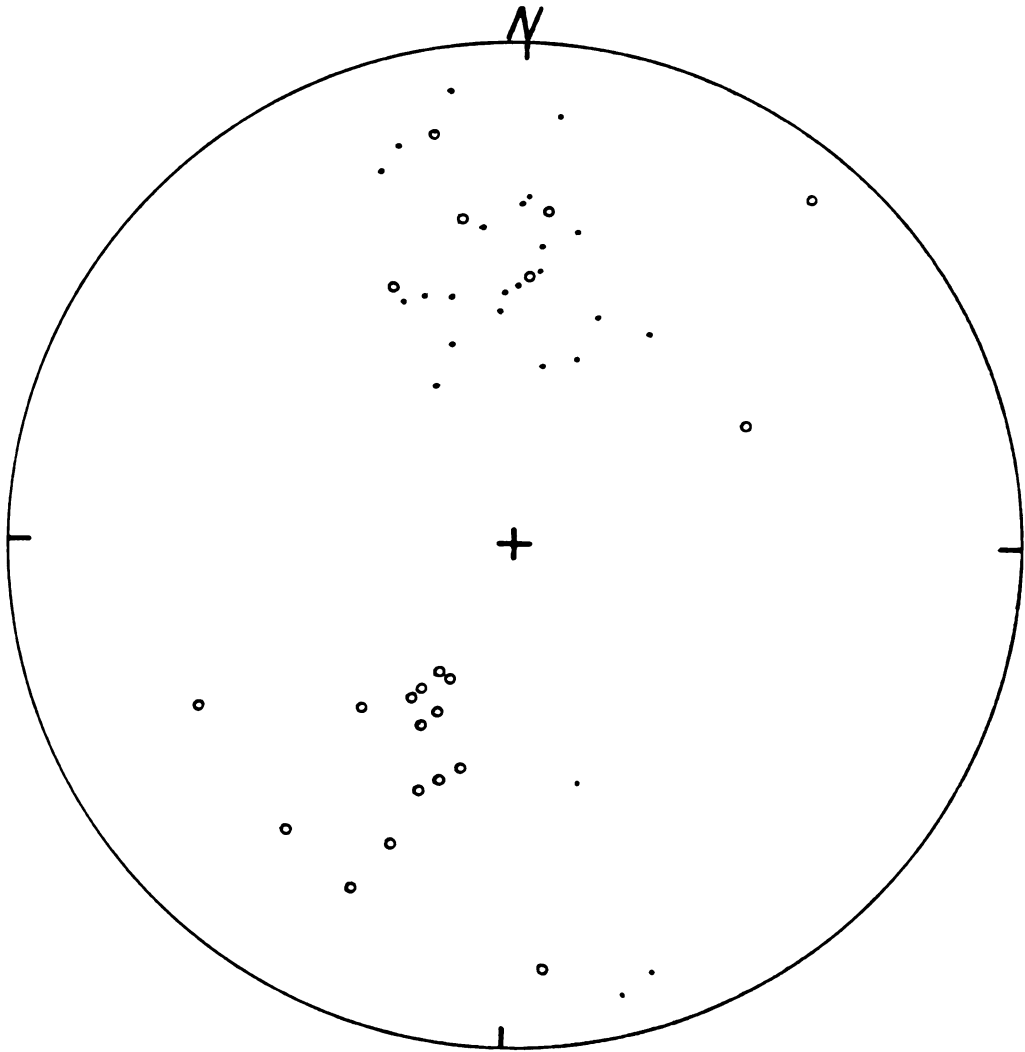


Figure 9b. Facepoles to the banding of the Mona Schist.



- = gneiss poles
- = Mona poles

Figure 10. Facepoles to foliation and banding.

they were deformed together, probably in the Algoman Orogeny approximately 2.5 bybp. However, there is a small but distinct difference in the foliation of the Mona and the tonalitic gneiss where the two units are in contact with one another. Structurally, this angular discordance and the distribution of facepoles could be explained by a set of east-west folds with nearly vertical axial planes in the Mona overlying a monocline in the gneiss (Figure 11). This model, which requires some very tight folds, is not the only one that is possible but it fits all the known evidence.

The foliations of the X-age metadiabase dikes are believed to have been formed during the Penokean Orogeny approximately 1.9 to 1.95 bybp. According to Berger (1971), the sheared margins and internal foliations of dikes can be used to establish the direction of maximum principle stress in an area if there are enough dike orientations available for a valid study. The 13 metadiabase dikes that show sheared margins and/or internal foliation are illustrated in Figure 12. It is felt that these dikes have enough different orientations to constitute a valid sample for determining the maximum stress direction. The stress direction that best fits the data available is N55°E (Figure 13). This is a significant departure from the north-south direction of compression that is generally given for the Penokean Orogeny.

To sum up the structural history of the area, then, it seems that it was deformed sometime before the deposition of the Mona Schist. The Mona was later intruded by a granite and then the entire area underwent north-south compression around 2.5 billion years ago. After a period of tension just prior to 2.0 billion years ago during which the X-age metadiabases were intruded, there was another compressional event that

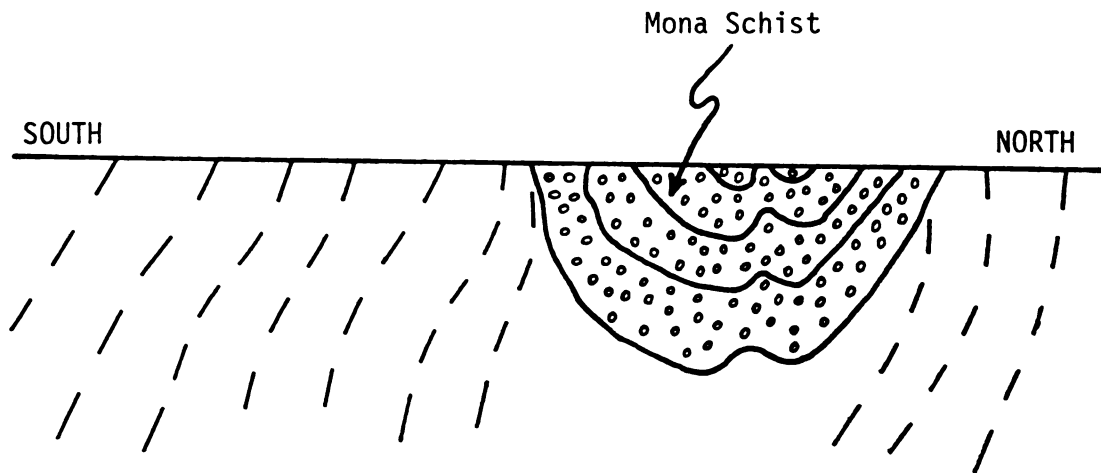


Figure 11. Structural cross-section through the study area

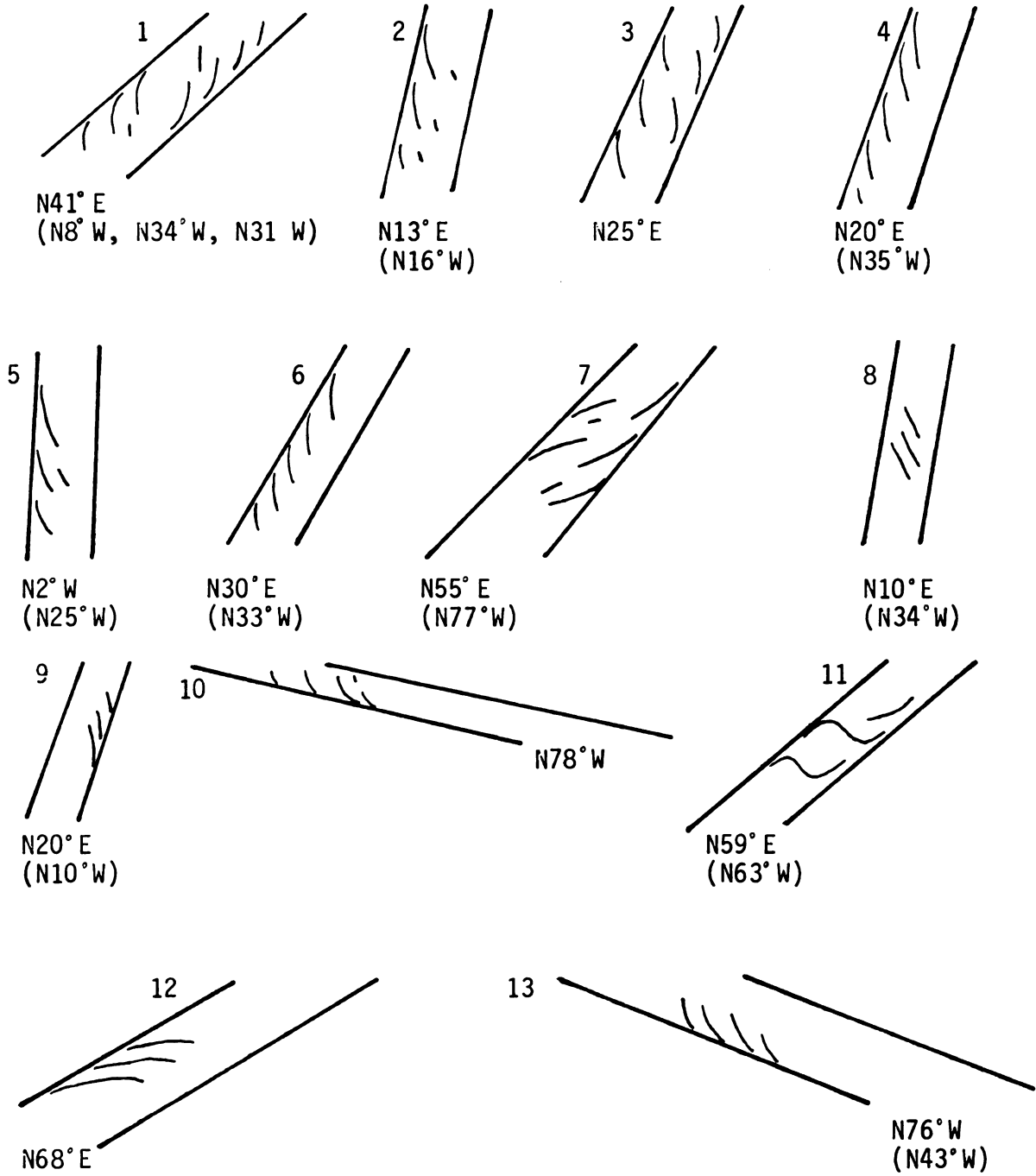


Figure 12. Foliation and shearing of X-age dikes (foliation direction in parentheses where measurable).

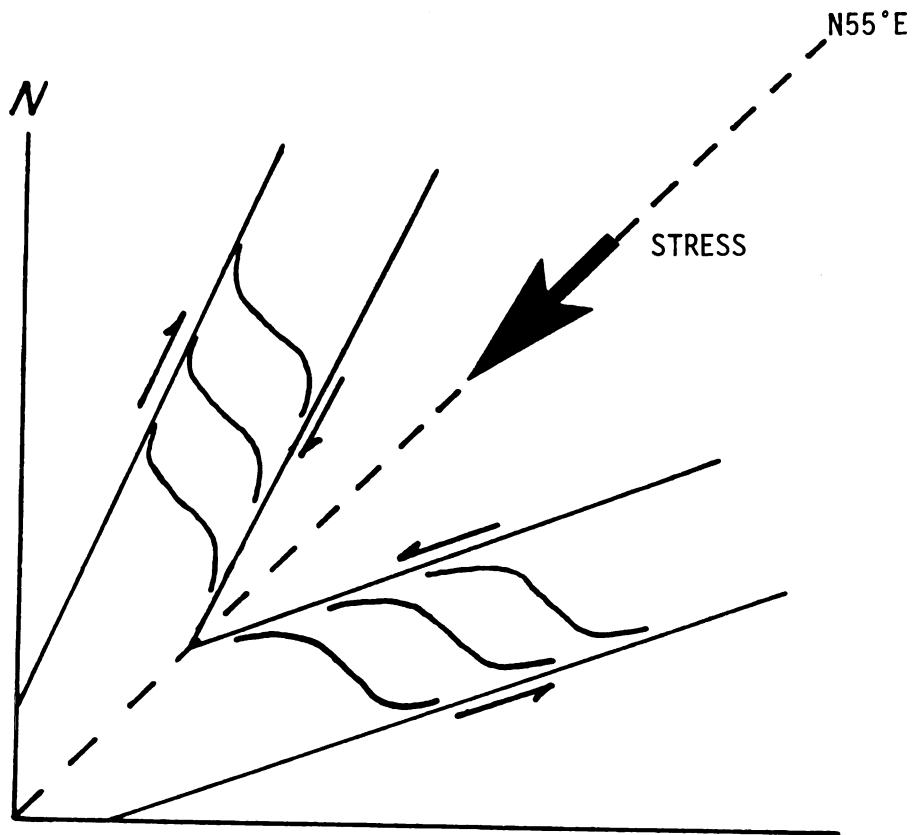


Figure 13. Model to explain the foliation and sheared margins of the metadiabase dikes.

acted along a northeast-southwest line which deformed the X-age dikes but had little or no effect on the W-age rocks present. The final deformational event in the area was another period of tension around 1.13 bybp during which the east-west trending Y-age diabase dike swarms were emplaced.

GEOPHYSICS

Interpretation

The first step in the interpretation process was to take the irregularly spaced magnetic data points and grid them. A resident computer program named GEOSYS (Wittick, 1974) was used to calculate the magnetic field values at each of the specified grid points from the original data using the local approximation method. All routines of this nature tend to smooth the original data and generate data for grid points where no field data were collected. Because of this, the GEOSYS grid was trimmed to reflect the distribution of the original data points. The steps used in data processing are outlined in Figure 14. The result of these procedures is shown in Figure 3.

As mentioned previously, the magnetic anomalies due to the Y-age diabase dikes tend to overwhelm the more modest anomalies due to the other rock units present in the area. Because of this, the next step in interpreting the data was to remove the effect of these dikes in order to see the magnetic expression of the other units more clearly. This was accomplished by preparing a second derivative map of the area using the computer program SHIFT (see Appendix A). The second derivative is used because it increases the magnitude of potential field anomalies. This enhanced map of the area (Figure 15) along with the original gridded data was used to locate the individual diabase dikes. An average susceptibility for the diabase dikes was then determined (Table 1) as well as an average natural remanent vector direction

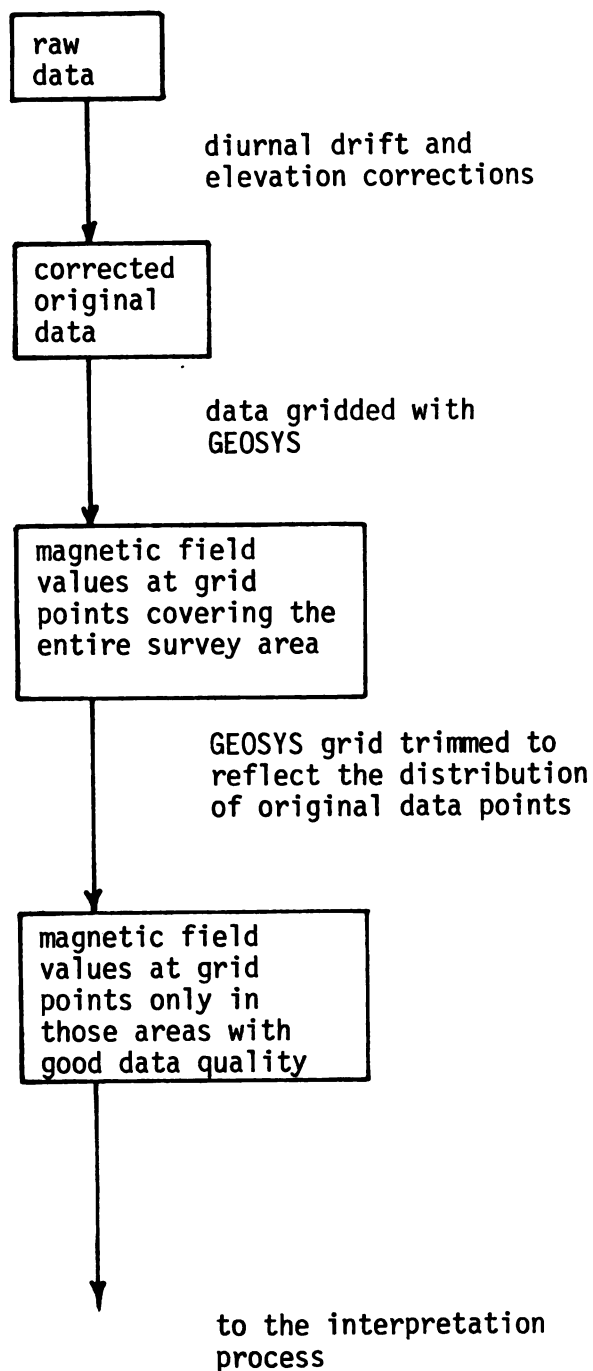


Figure 14. Data processing procedures.

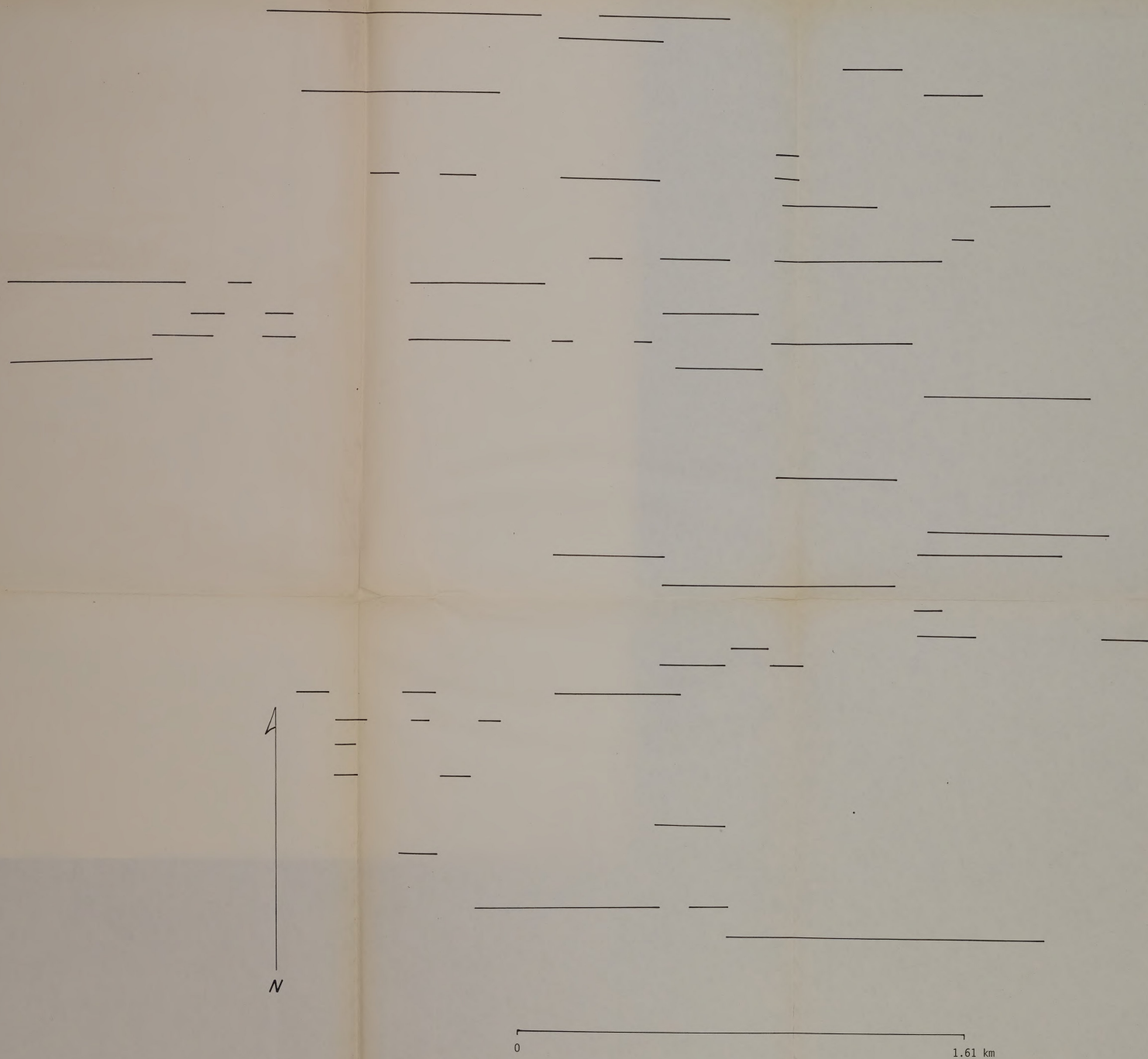


Figure 15. Traces of linear lows from the second derivative map.

Table 1. Average magnetic susceptibility of the various rock units studied in cgs units.

rock type	number of samples	average susceptibility(k)	range of k values high	low
diabase	14	0.00327	0.00368	0.00268
gneiss	13	0.000004	0.000008	0.000000
Mona Schist	8	0.000007	0.000010	0.000005
X-age metadiabase	11	0.000027	0.000045	0.000014
metadiabase of uncertain age	5	0.00754	0.00881	0.00606

(Table 2). This information as well as the location of the dikes was then processed by a computer program named SHALOCI (see Appendix A). This computer program calculates the magnetic field due to the dikes at each of the grid points and these values are shown in Figure 16. These values were then subtracted from the original gridded data values to remove the effect of the Y-age diabase dikes (Figure 17). This "residual map" was then used to interpret the area in terms of rock types other than the Y-age diabase.

From Figure 5, it can be seen that there are four diabase dike swarms in this area. These swarms correlate very well with the outcrops of Y-age diabase that were mapped. The correlation would probably be better if the magnetic data density was increased in some areas but the agreement is still good enough to lend credibility to the projected dikes that occur in areas that have no outcrop control.

Figure 7 shows the correspondence between the residual highs from Figure 17 and the known outcrops of metadiabase. The correlation between the two is very good since every major outcrop of metadiabase, and even some of the smaller ones, has a positive anomaly associated with it. On the strength of this fact, it would seem reasonable to believe that each of the other positive anomalies shown on Figure 7 is in fact the magnetic expression of an unmapped metadiabase body.

The residual map (Figure 17) also indicates a sharp decrease of about 300 gammas in the vertical magnetic field's strength as one goes into the northeast corner of the map. This decrease in field strength occurs very close to the contact between the gneiss and the Mona Schist in areas where the position of this contact is known. As a result, this sharp change in the character of the observed magnetic field seems

Table 2. Comparison of paleomagnetic data.

area/source	type of cleaning	position of S-seeking pole	declination	inclination	95	k_{Fisher}	number of samples
this study	AC	150.3W, 43.6N	112.2	-62.5	1.6	1042	9
this study	thermal	145.7W, 41.4N	109.7	-61.3	2.4	424	10
Duluth gabbro and Logan diabase/ Beck (1970)	AC	156.5W, 42.5N	91.0	-65.5	6.0		13
Baraga Co. dikes/ Graham (1953)	AC	99.5W, 45N					
Grand Portage/ Books (1968)	AC	163W, 44N	117.0	-59.2	4.0	129	11
Logan sills/ Robertson and Fahrig (1971)	AC	140W, 47N	107.0	-72.0	8.0	34	51
Logan sills/ Palmer (1970)	AC	141.7W, 48.4N	109.0	-71.2	5.0	53	30

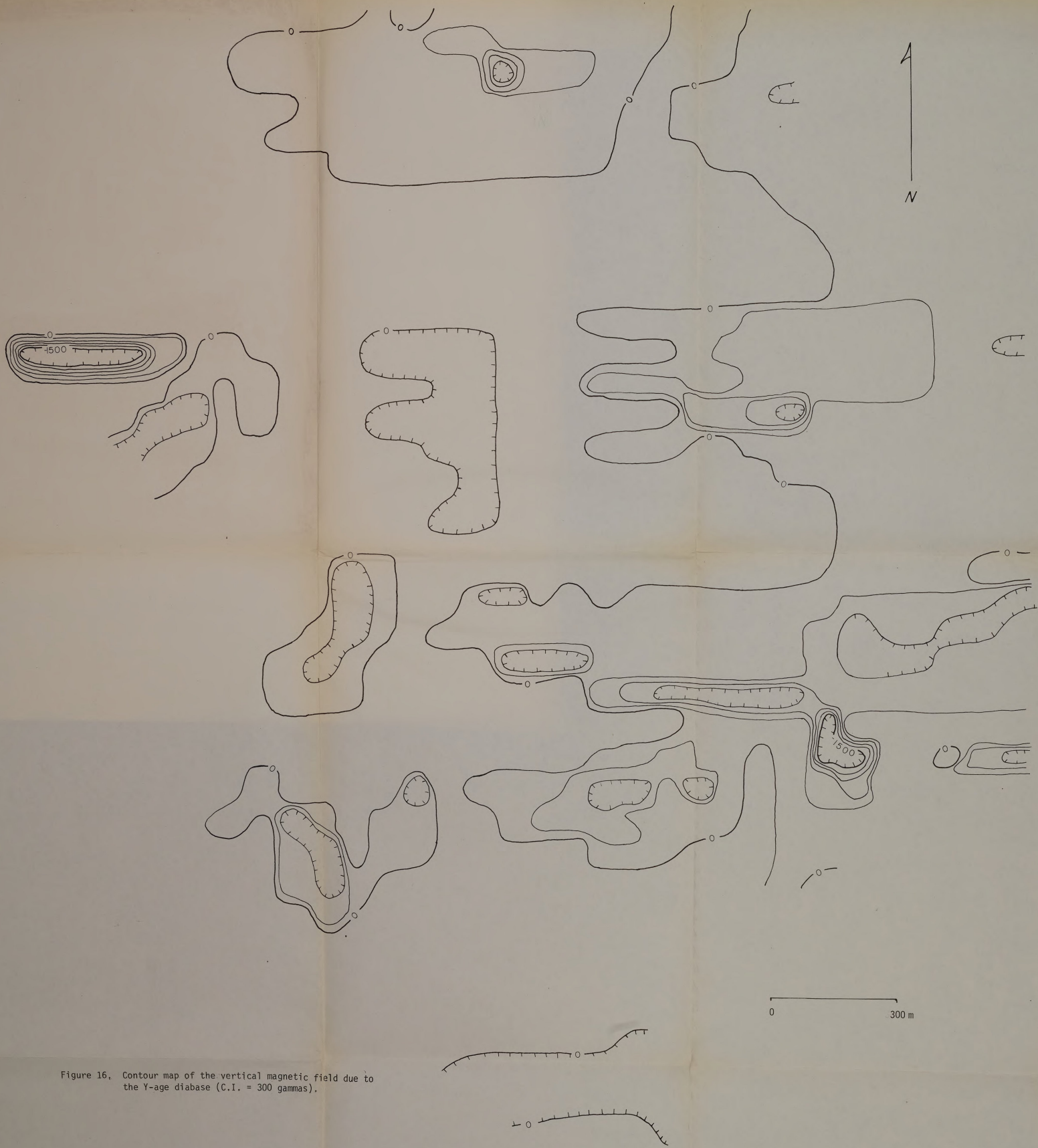


Figure 16. Contour map of the vertical magnetic field due to the Y-age diabase (C.I. = 300 gammas).

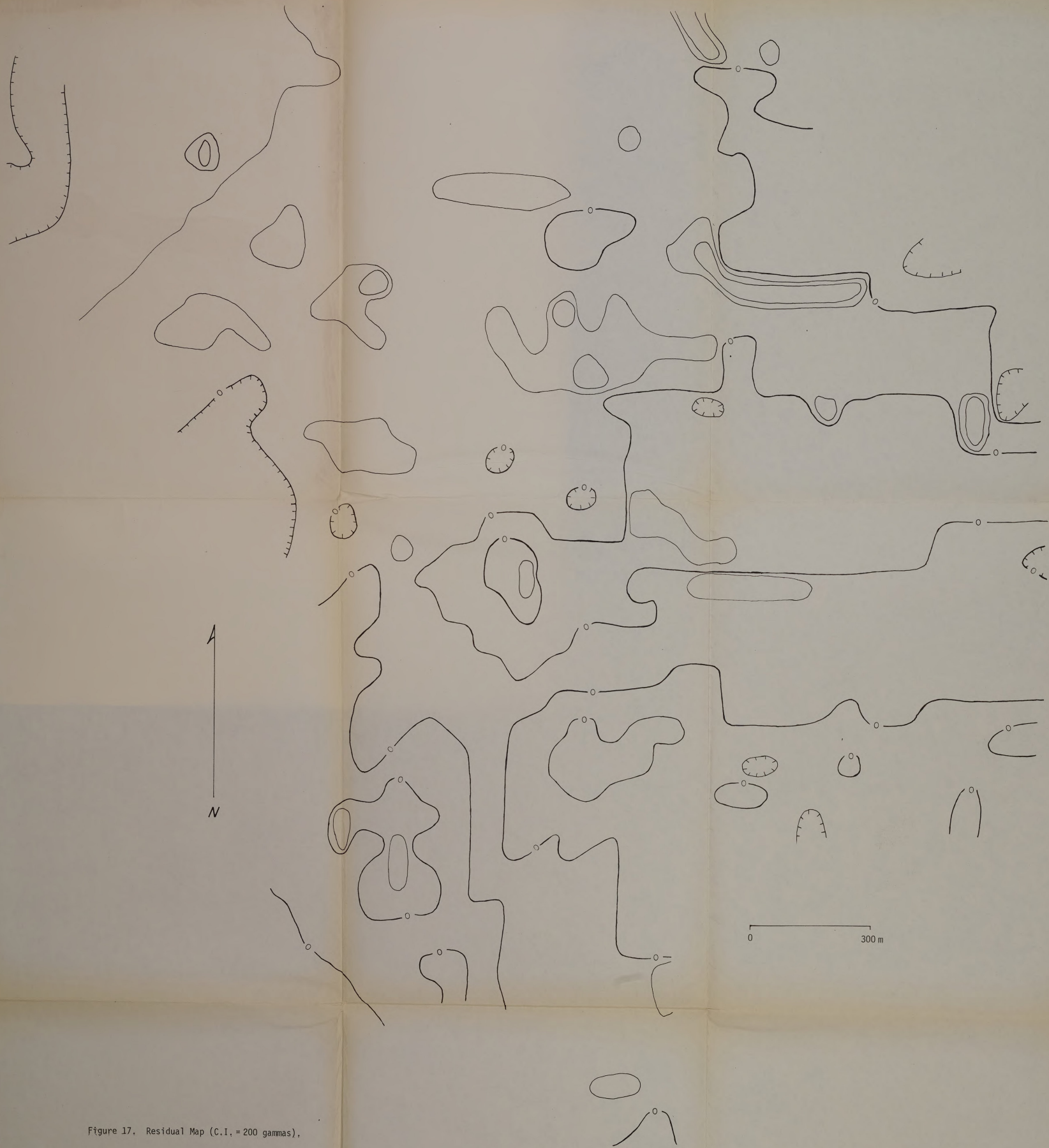


Figure 17. Residual Map (C.I. = 200 gammas),

to be a good way of establishing the gneiss/Mona Schist contact in areas where its exact location is not known. This difference between the magnetic character of the gneiss and the amphibolite is also interesting in that since their susceptibilities are almost identical (Table 1), this difference must be due either to a radical difference in the strengths of their natural remanent vectors or to a substantial difference in the orientations of their natural remanent vectors.

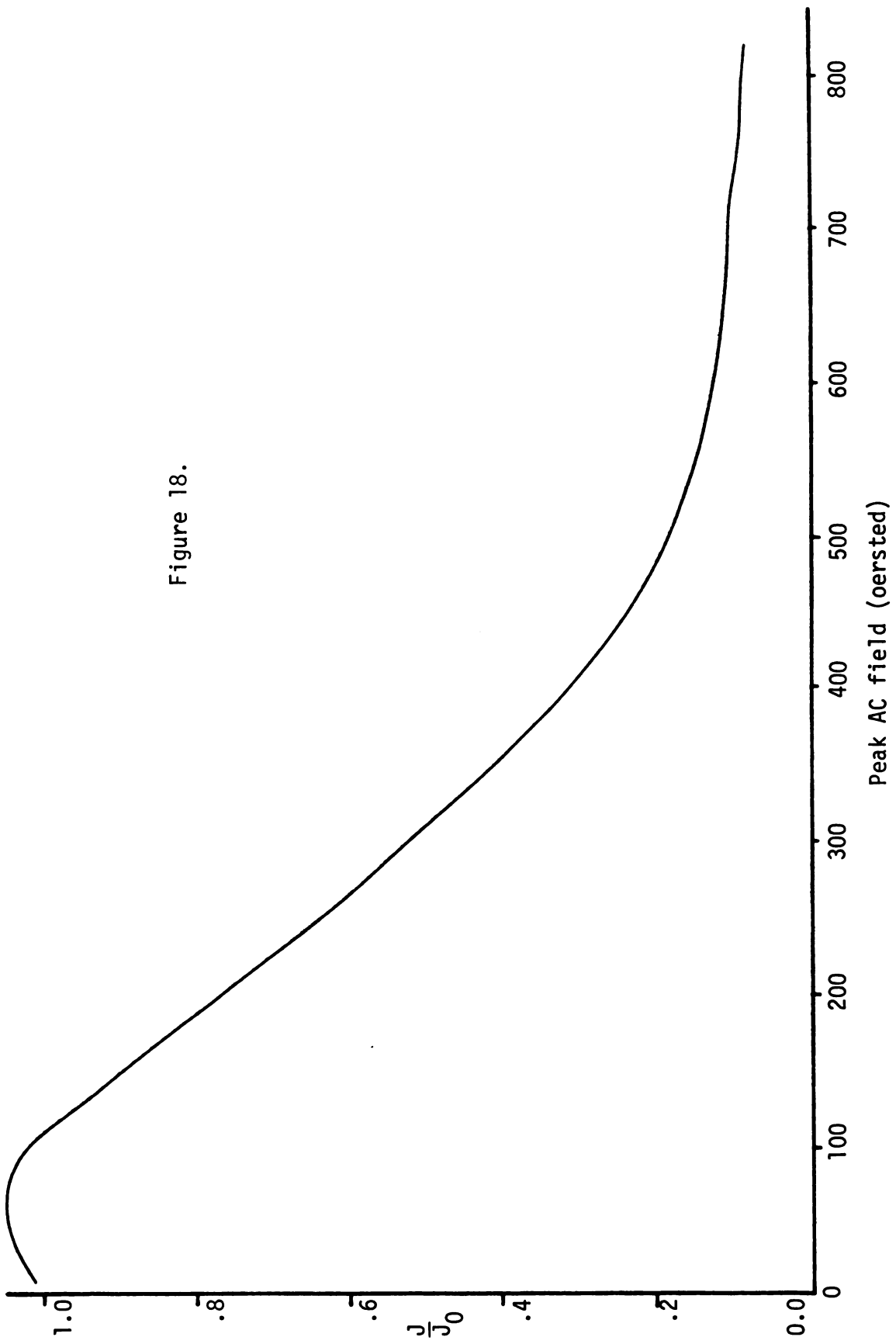
Paleomagnetism

Oriented specimens cored from blocks of Y-age diabase and X-age metadiabase were analyzed by the author in the Paleomagnetism Laboratory at the University of Michigan. Nine samples of the Y-age diabase were cleaned using the alternating field method while ten others were cleaned thermally. Ten samples of metadiabase were also cleaned thermally but there was an equipment failure before the analysis was complete.

The natural remanent field of the Y-age diabase is extremely strong and it seems to have only a small component due to isothermal or viscous effects as can be seen from the shape of the AC demagnetization curve (Figure 18) and the straight-line nature of the Zijderveld diagram (Figure 19) (McElhinny, 1973). Because of this fact, AC and thermal cleaning do not enhance the clustering of the samples' poles by a noticeable factor although the thermal cleaning does seem to improve the grouping more than the AC cleaning (Figures 20a, 20b, 21a, and 21b). Since heating to 150°C or exposure to an AC field of 100 oersteds seems to be sufficient to remove any secondary magnetic components, the samples' declination and inclination values at this stage of demagnetization were used to calculate an average paleopole position (Table 3)

Figure 18. AC demagnetization curve for Y-age diabase samples.

Figure 18.



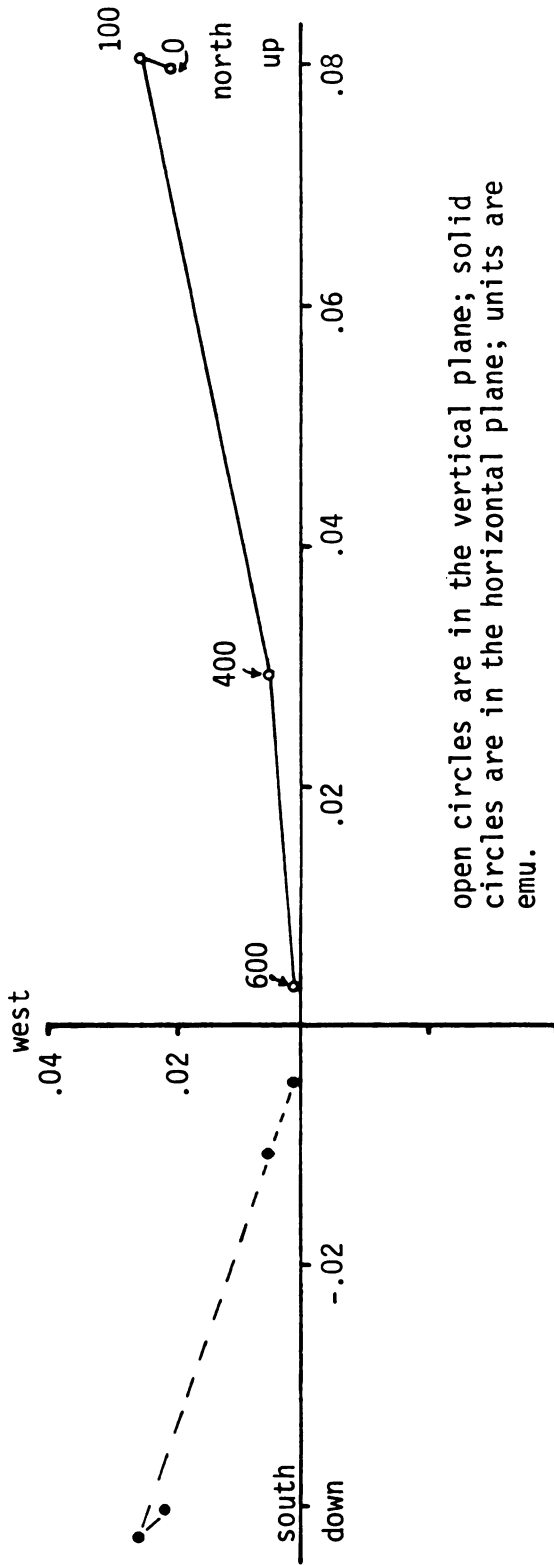
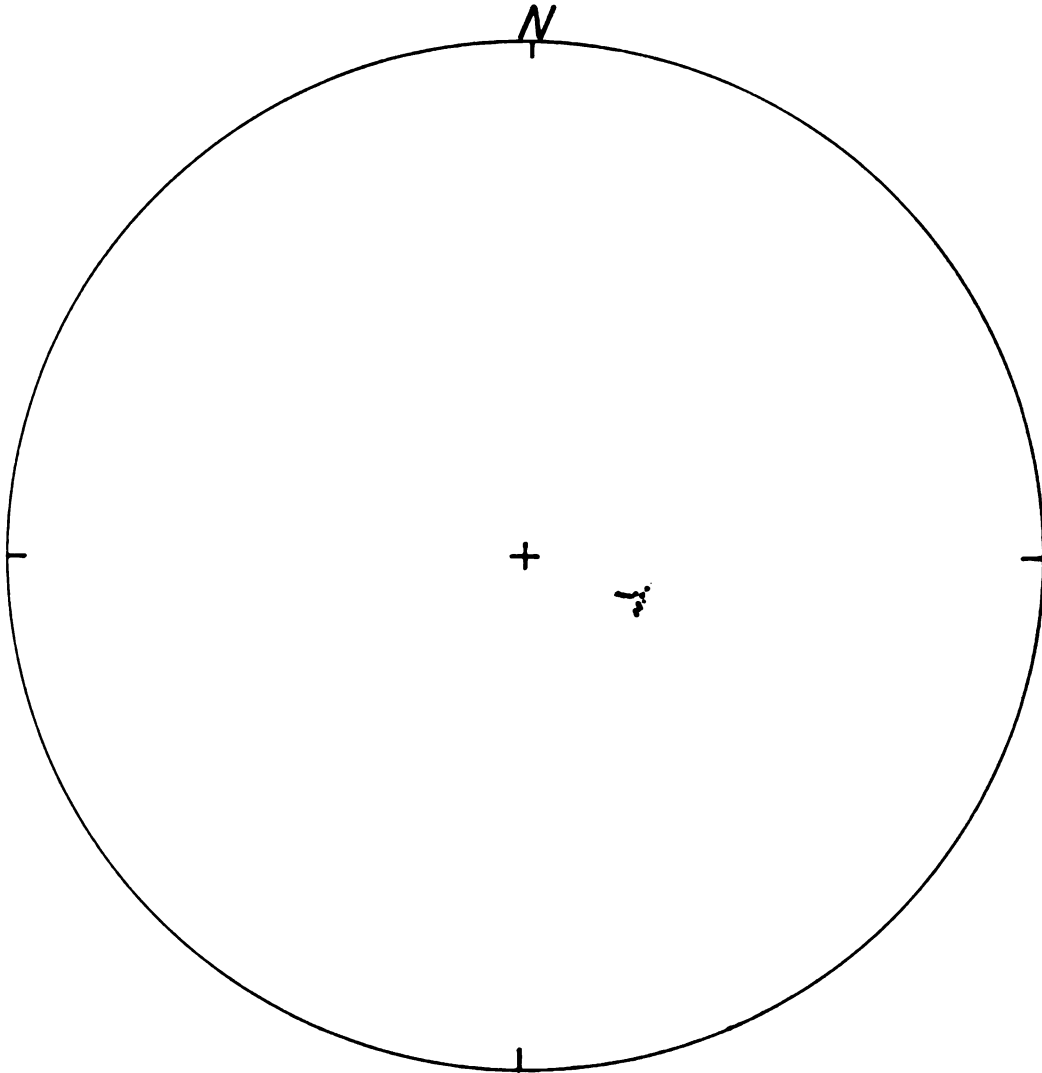
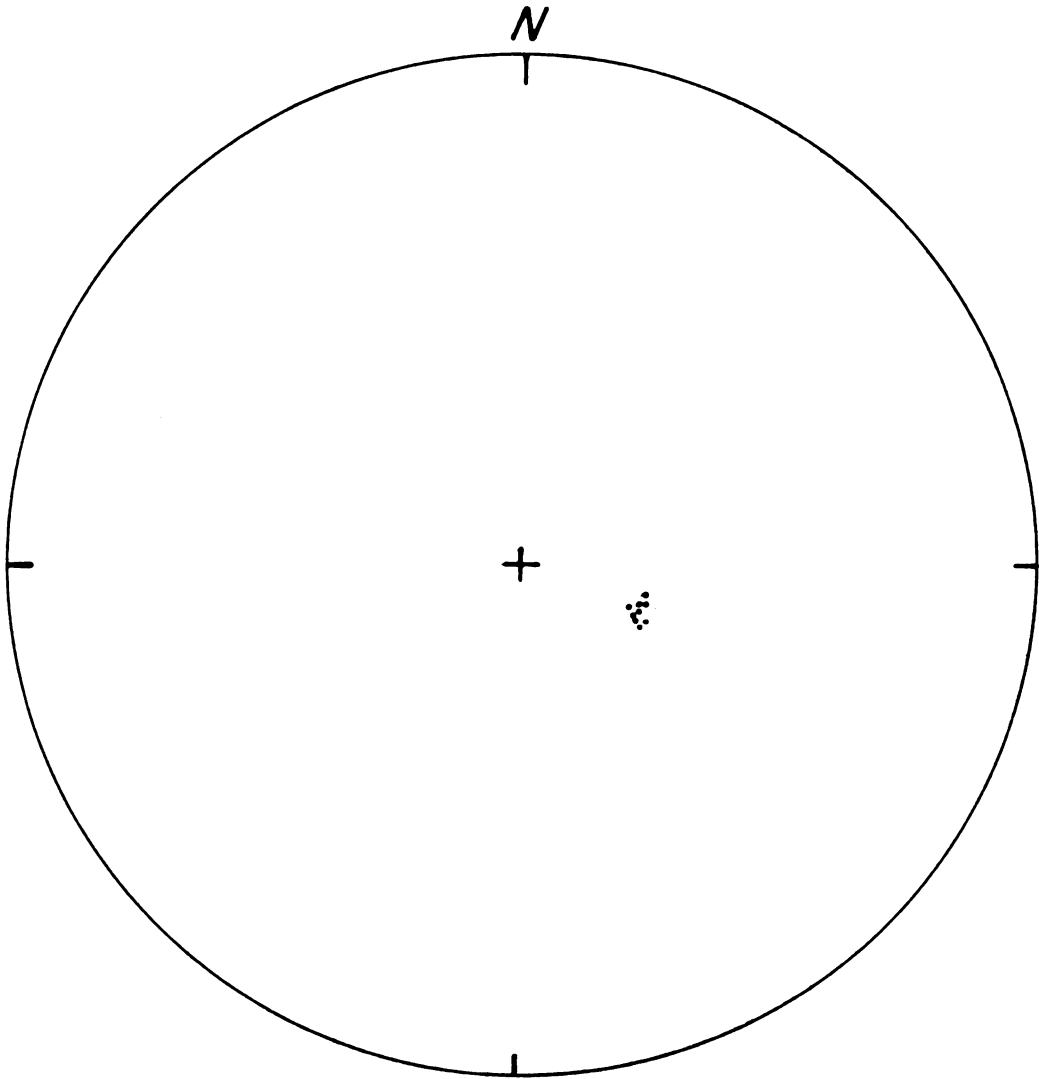


Figure 19. A typical AC-demagnetization (sample 12A2H) with peak AC field in oersteds given.



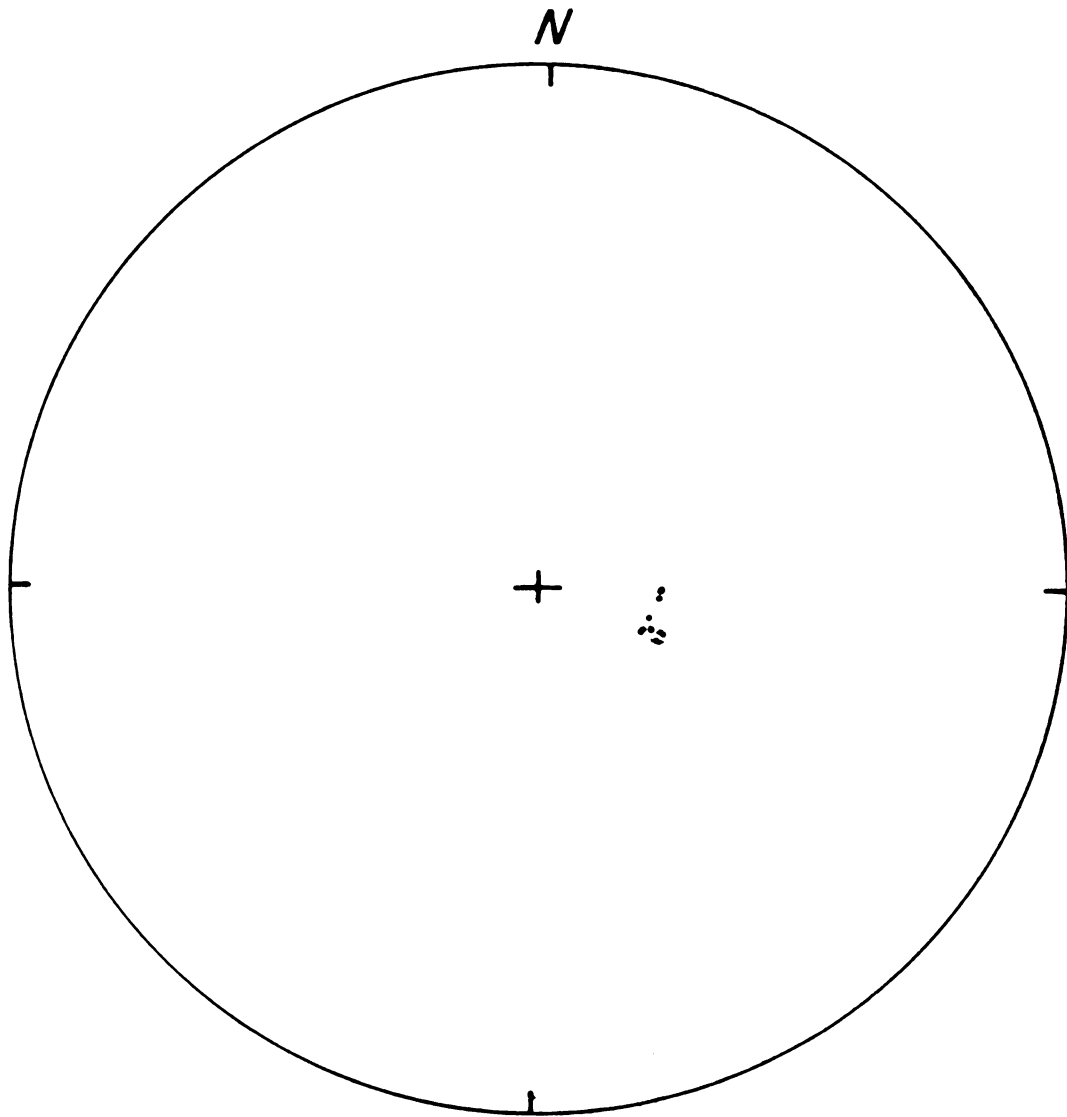
• = poles, all out of stereonet

Figure 20a. Y-age diabase pre-AC cleaning.



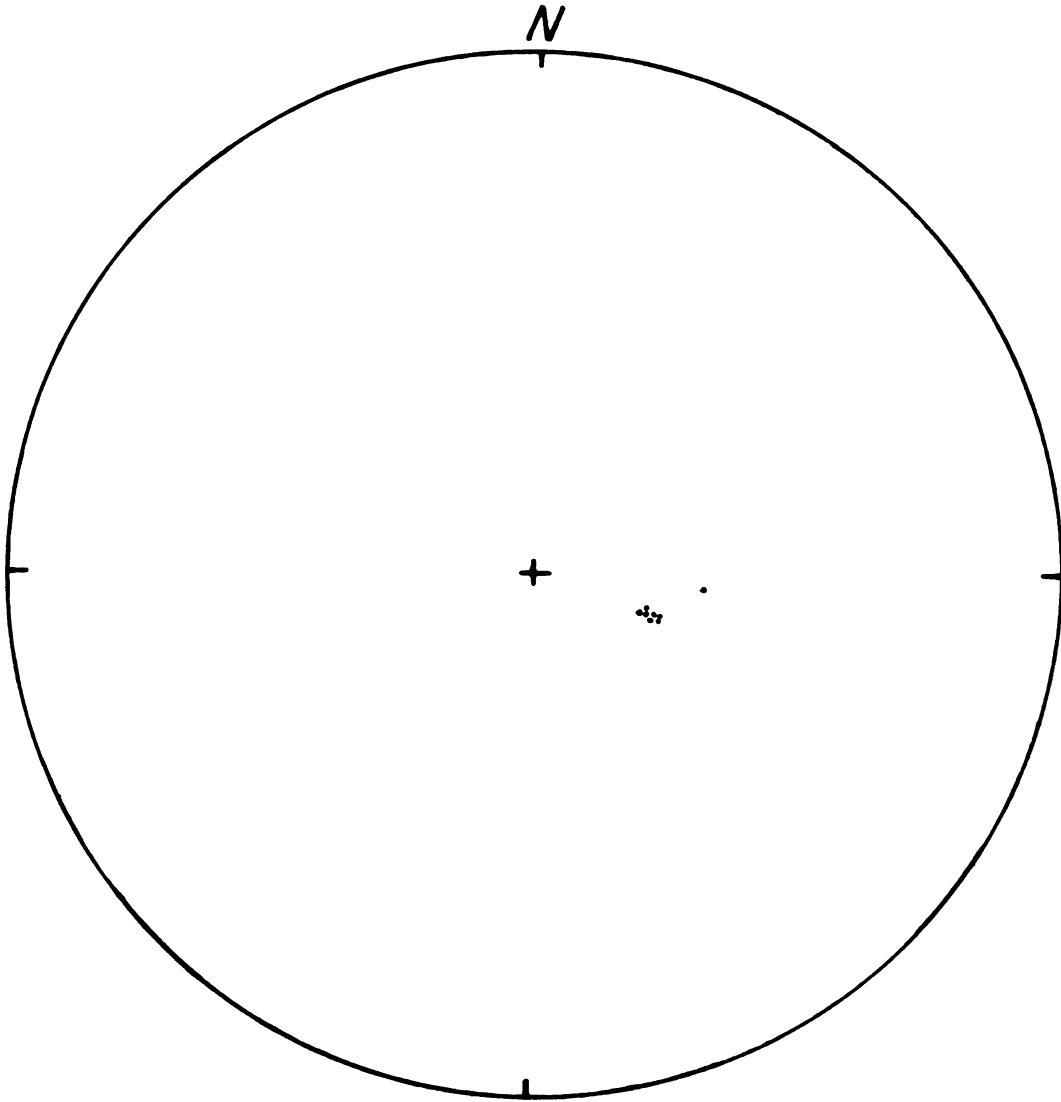
• = poles, all out of stereonet

Figure 20b. Y-age diabase cleaned in AC field of 100 oe.



• = poles, all out of stereonet

Figure 21a. Y-age diabase pre-thermal cleaning.



• = poles, all out of stereonet

Figure 21b. Y-age diabase thermally cleaned (150°C).

Table 3. Data used in determining Y-age paleopole.

100 oc AC field cleaning (values in emu times 10¹)

<u>sample</u>	<u>x</u>	<u>y</u>	<u>z</u>
12A2P	-.1110	.4450	-.8886
12A2G	-.1796	.4170	-.8910
12A2C	-.1469	.4443	-.8838
12A2M	-.1290	.4091	-.9033
12A2H	-.2125	.4357	-.8746
12A2J	-.2276	.4281	-.8746
12A2K	-.1900	.4002	-.8965
12A2D	-.1597	.4365	-.8854
12A2R	<u>-.2066</u>	<u>.4199</u>	<u>-.8838</u>
	-1.5629	3.8358	-7.9816

$$x_{\text{average}} = -.1737 \quad y_{\text{average}} = .4262 \quad z_{\text{average}} = -.8868$$

Average declination = 112.17
 Average inclination = -62.47

Location of South-seeking pole = 150.3°W, 43.6°N

150°C thermal cleaning (values in emu times 10¹)

<u>sample</u>	<u>x</u>	<u>y</u>	<u>z</u>
12A2L	-.1939	.4275	-.8829
12A2A	-.0679	.5867	-.8070
12A2Q	-.1864	.4591	-.8686
12A2O	-.1561	.4130	-.8973
12A2F	-.1506	.4398	-.8854
12A2N	-.1656	.4160	-.8942
12A2I	-.1647	.3995	-.9018
12A2E	-.1727	.4456	-.8738
12A2S	-.1614	.4458	-.8804
12A2T	<u>-.1835</u>	<u>.4388</u>	<u>-.8796</u>
	-1.6028	4.4808	-8.7710

$$x_{\text{average}} = -.1603 \quad y_{\text{average}} = .4481 \quad z_{\text{average}} = -.8771$$

Average declination = 109.68
 Average inclination = -61.29

Location of South-seeking pole = 145.7°W, 41.1°N

using the method outlined by Tarling (1971). These Y-age paleopoles meet the criteria of reliability set forth by McElhinny (1973) and agree with each other at the 99 percent confidence level. When compared with other paleopoles from this time period (Table 2), the paleopoles fall between the pole from the Logan sills and the pole from the Duluth gabbro and the Logan diabase in the center of the reversed magnetic period of the middle Keweenawan. When plotted on the apparent polar wandering track constructed by Irving and McGlynn (1976) they fall near the center of Track 3A, suggesting an age of about 1.12 to 1.13 bybp (Figure 22). This agrees well with the date of 1.14 bybp given by Chase and Gilmer (1973) for the beginning of rifting associated with the formation of the Keweenawan Trough in the Lake Superior region of North America.

Due to the conflicting nature of the results from the partially demagnetized metadiabases, no paleopoles were calculated for these samples although the data are included in Appendix C. The only conclusion that can be safely drawn from these data is that the natural remanent vectors of the metadiabase samples, even within a single rock body, are close to being randomly oriented (Figure 23). This means that the positive magnetic anomalies associated with the metadiabases are probably due to induced magnetization alone since the randomly oriented natural remanent vectors would tend to cancel each other out.

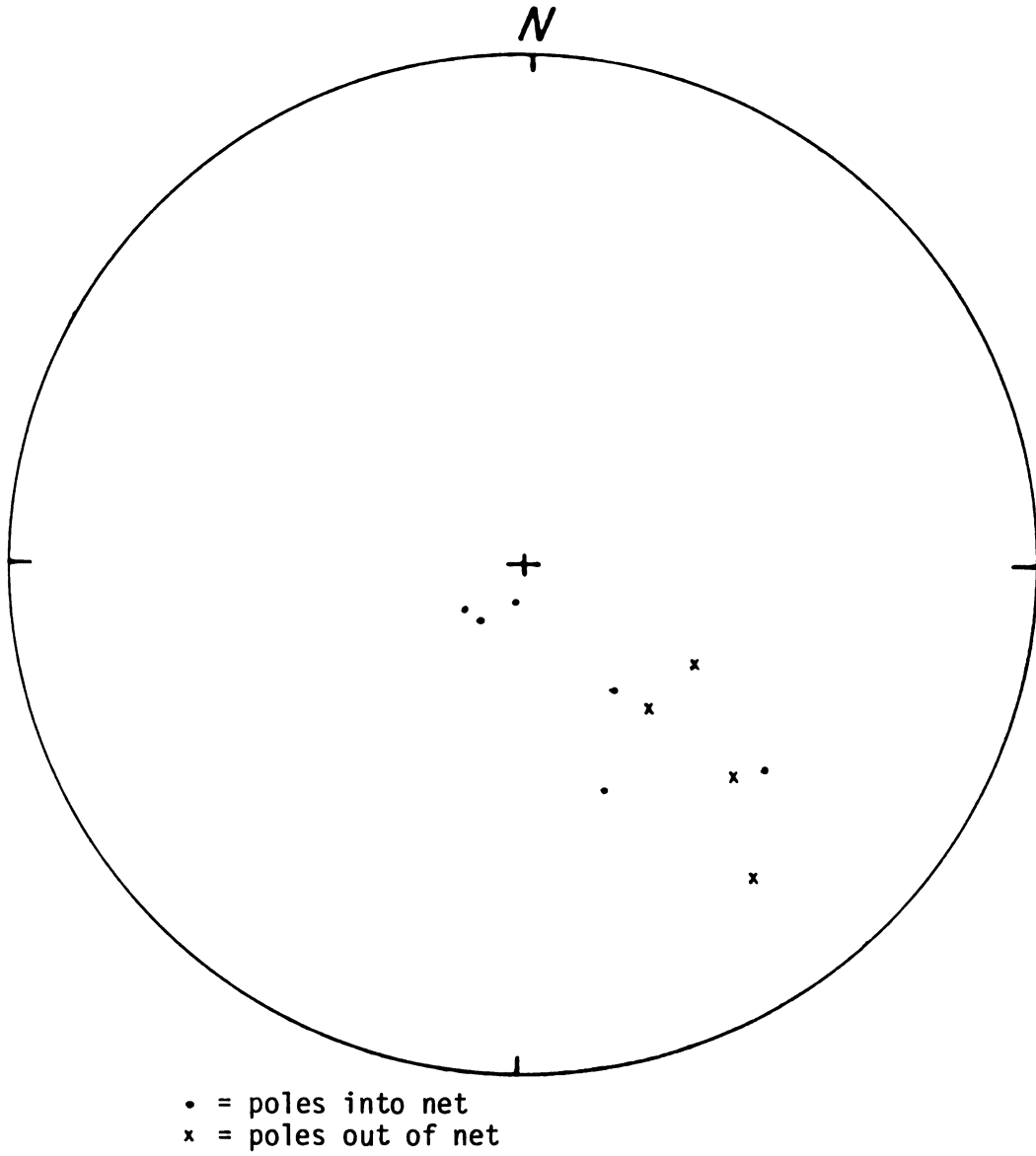
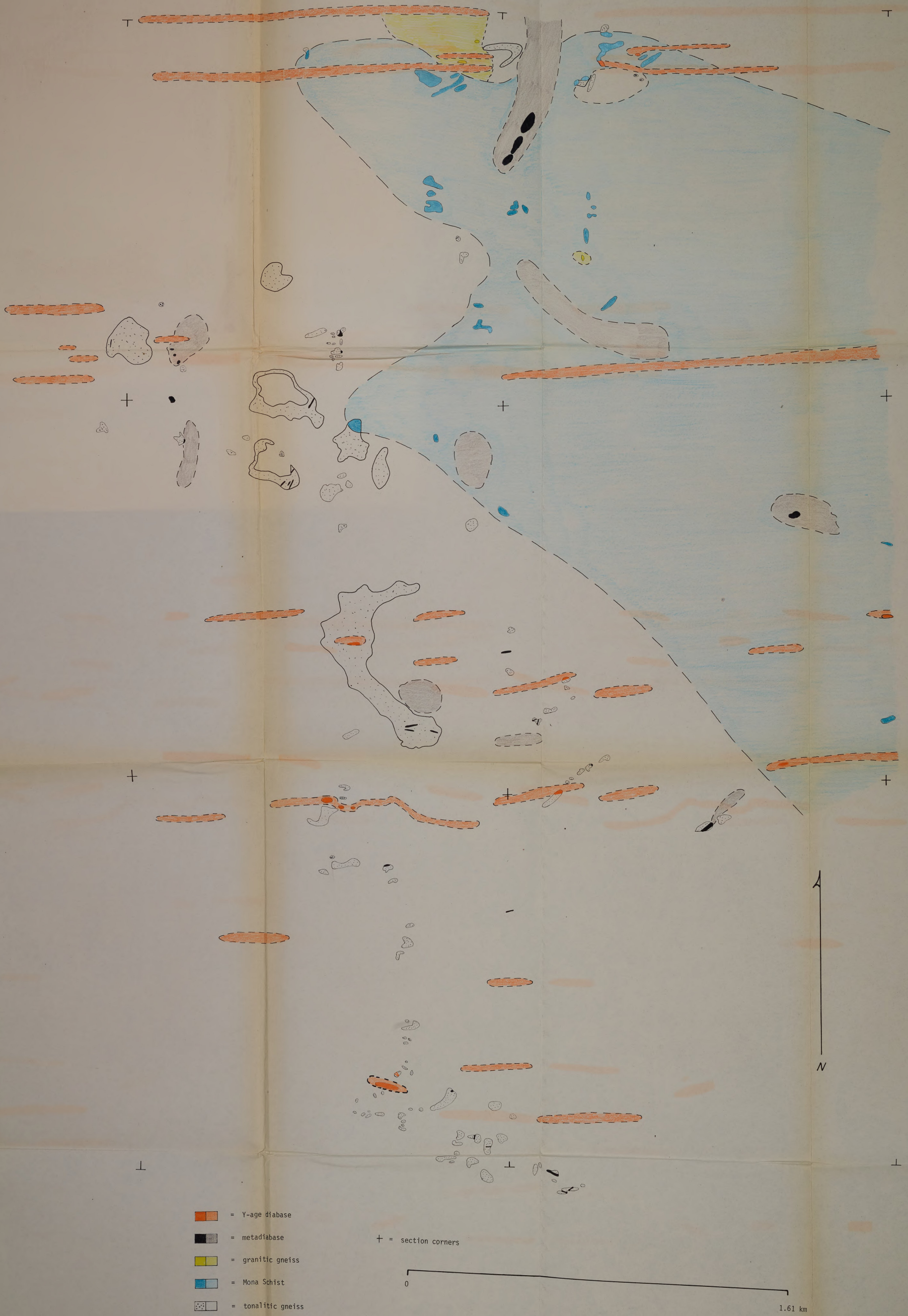


Figure 23. NRM directions of X-age metadiabase.

DISCUSSION AND CONCLUSIONS

Combining the information supplied by the interpretation of the ground magnetic survey with that derived from field geology and thin section work a geological map of the area was drawn (Figure 24). The sequence of events that led to the present pattern is believed to be as follows:

- (1) The intermediate volcanics of the Mona Schist are deposited on top of an already deformed tonalitic gneiss.
- (2) The Mona and the gneiss are deformed together in the Algoman Orogeny to form a series of folds with east-west, vertically dipping axial planes.
- (3) During the later stages of this orogeny, a granite intruded the area. This granite was mildly deformed to form a granitic gneiss.
- (4) After a period of quiescence, the area was subjected to tensional stress during which at least two sets of Precambrian X-age gabbros and diabases were emplaced. This event may coincide with the opening of the Marquette Trough.
- (5) During the compression associated with the Penokean Orogeny, the X-age gabbros and diabases were metamorphosed to Greenschist facies. Some of these basic rocks developed internal foliations and sheared margins during this event which indicate that the



- = Y-age diabase
- = metadiabase
- = granitic gneiss
- = Mona Schist
- = tonalitic gneiss

+ = section corners

0 1.61 km

Figure 24. Geologic map of the study area.

compressive stress acted on a northeast-southwest line.

(6) After another period of inactivity, the area was again subjected to tensional stress during which several swarms of east-west trending Keweenawan diabase dikes were emplaced.

As noted before, the evidence for folding in this area is not conclusive. However, it seems to be the best solution that is possible at the present time. Any other model that explains the present structural picture requires a complex folding or thrusting of the Mona Schist into the older basement complex for which there is no evidence at the present time. It is possible, of course, that the amphibolite in this area is not part of the Mona Schist at all but rather an amphibolitic subunit or inclusion in the gneiss. However, the fact that no large amphibolitic members of this nature in the gneiss have been reported, and the distinct difference in magnetic character of the two rock types would tend to argue against this. It would seem more reasonable, then, to accept the idea advanced here of equating the amphibolite with part of the Lighthouse Point Member of the Mona Schist.

The computer-aided interpretation of the magnetic data fits the known geologic data very well. It is probable that some error was introduced by using GEOSYS to grid the data before SHALOCI was used to construct a geologic model. Most of this error was probably removed, however, by deleting the grid values for areas in which there were no original magnetic observations. The fit of the computer model to the actual geology could have been improved if magnetic observations had been made in these areas. Nevertheless, it seems clear that it is

possible to use gridded magnetic data and computer-aided interpretation to project structure and rock types from known into unknown areas, even in complex Precambrian terranes. Further, it also appears that it is feasible to use these same types of techniques to determine the orientation of a body's natural remanent magnetic vector (Appendix B). This vector orientation can then be used to help determine a body's relative and absolute age if the polar wandering path for that period in that area is well defined as a means of comparing two or more geologic units.

The results of the paleomagnetic analyses done on the Precambrian Y-age dikes in this area yield a South-seeking paleopole at Longitude 148°W , Latitude 42.5°N . This pole has an age of 1.13 bybp according to the apparent polar wandering path of Irving and McGlynn (1976) which would place these basic intrusives in the lower middle Keweenawan (Chase and Gilmer, 1973).

Due to poor data quality and lack of equipment, it proved impossible to thoroughly analyze the X-age metadiabase samples paleomagnetically, but the information that was gathered indicates that the natural remanent magnetic vectors of these samples are somewhat randomly oriented. This means that the magnetic highs associated with these rock bodies are probably due entirely to induced magnetic fields. More paleomagnetic work will have to be done, however, before this interesting conclusion could be used to help interpret magnetic data in other areas in the Upper Peninsula of Michigan.

In conclusion, it seems clear that computer-aided interpretation of magnetic data using SHALOCI is a viable method for extending the geology of mapped areas into unexplored territory regardless of the

complexity of the geology. The SHALOCI method represents an advance in magnetic interpretation techniques in that it takes into account the often substantial magnetic field caused by a body's natural remanent magnetic vector which has largely been ignored in the past. It is hoped that this method will prove to be a useful tool in the future by making quicker and more accurate interpretations of magnetic data from a variety of geologic areas available.

APPENDICES

APPENDIX A

Description of Computer Programs

Two computer programs were used in interpreting the magnetic data gathered for this thesis. The magnetic modeling was done with the aid of SHALOCI, a new program written by William Ciolek, Mark Locher, and the author (hence the name SHA-LO-CI). A complete listing of this Fortran program is given at the end of the program description below in Table 4. Downward continuation and derivatives of the data were made with SHIFT, a modified version of HNDRSN2 which is used for potential field analysis by the Indiana Geological Survey. A short description of it and the theory behind it will be given below. The reader is referred to the comprehensive paper by Rudman and Blakely (1975) for further details.

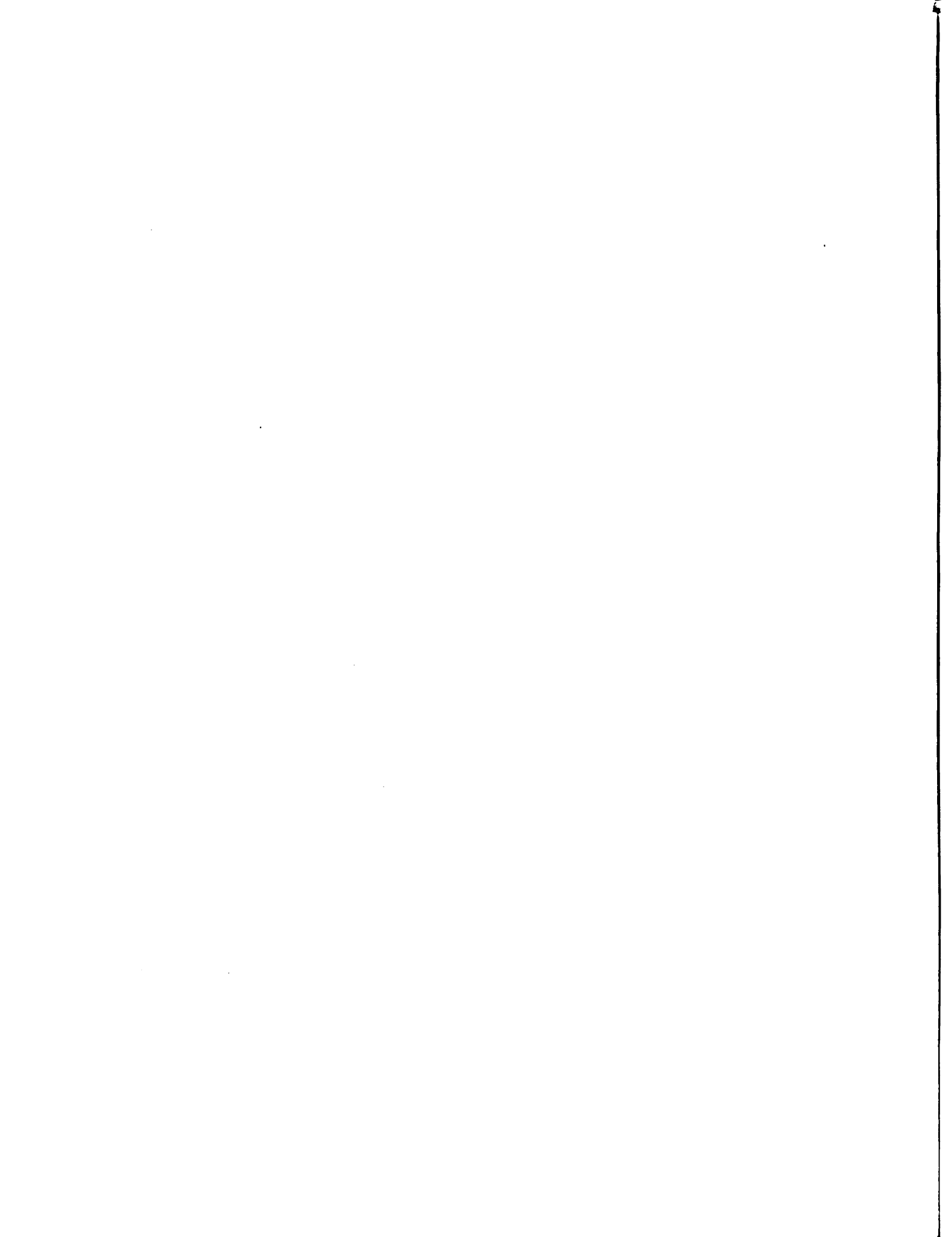
SHALOCI is a two or three dimensional magnetic modeling program. It calculates the vertical magnetic anomaly produced by buried prisms with varying magnetic properties using a modified version of the equation discussed by Whitehill (1973). SHALOCI makes use of the equation:

$$H_z(x,y,z) = I_p \left[\frac{M}{2} \log \left(\frac{r+u}{r-u} \right) + \frac{L}{2} \log \left(\frac{r+v}{r-v} \right) - N \tan^{-1} \left(\frac{uv}{rw} \right) \right] \begin{vmatrix} u_1 & v_1 & w_1 \\ u_0 & v_0 & w_0 \end{vmatrix}$$

where: $H_z(x,y,z)$ is the vertical magnetic field due to a prism $(x_0, y_0, z_0; x_1, y_1, z_1)$ at a point (x,y,z)

I_p is the intensity of magnetization of the prism

$L, M,$ and N are the direction cosines of I_p



$$r = \sqrt{u^2 + v^2 + w^2}$$

$$u_0 = x_0 - x \quad u_1 = x_1 - x$$

$$v_0 = y_0 - y \quad v_1 = y_1 - y$$

$$w_0 = z_0 - z \quad w_1 = z_1 - z$$

(see Figure 25)

This equation was first derived by Bhattacharyya (1964) and adequately accounts for the induced magnetic field of the body when:

$$\vec{I}_p = k \cdot \vec{F}$$

where k is the prism's magnetic susceptibility and \vec{F} is the earth's magnetic field. The authors of SHALOCI, however, have chosen not to neglect remanent magnetization so now:

$$\vec{I}_p = k \cdot \vec{F} + \vec{J}_{\text{NRM}}$$

where \vec{J}_{NRM} is the prism's natural remanent magnetic vector. It is this feature that sets SHALOCI apart from most existing magnetic modeling programs since it makes SHALOCI one of the few magnetic modeling programs available that treats remanent magnetism in a meaningful and straightforward manner.

The computer program SHIEK used in Appendix B of this thesis is exactly like SHALOCI in all respects except that it makes use of the additional equations:

$$H_x(x,y,z) = I_p \left[\frac{N}{2} \cdot \log\left(\frac{r+v}{r-v}\right) + M \cdot \log(r+w) + L \cdot \tan^{-1}\left(\frac{uv}{u^2+v^2+w^2}\right) \right] \begin{vmatrix} u_1 & v_1 & w_1 \\ u_0 & v_0 & w_0 \end{vmatrix}$$

$$H_y(x,y,z) = I_p \left[\frac{N}{2} \cdot \log\left(\frac{r+u}{r-u}\right) + L \cdot \log(r+w) + M \cdot \tan^{-1}\left(\frac{uv}{r^2+rw-u^2}\right) \right] \begin{vmatrix} u_1 & v_1 & w_1 \\ u_0 & v_0 & w_0 \end{vmatrix}$$

$$\text{and } T(x,y,z) = l \cdot H_x(x,y,z) + m \cdot H_y(x,y,z) + n \cdot H_z(x,y,z)$$

where l , m , and n are the direction cosines of the earth's field, in

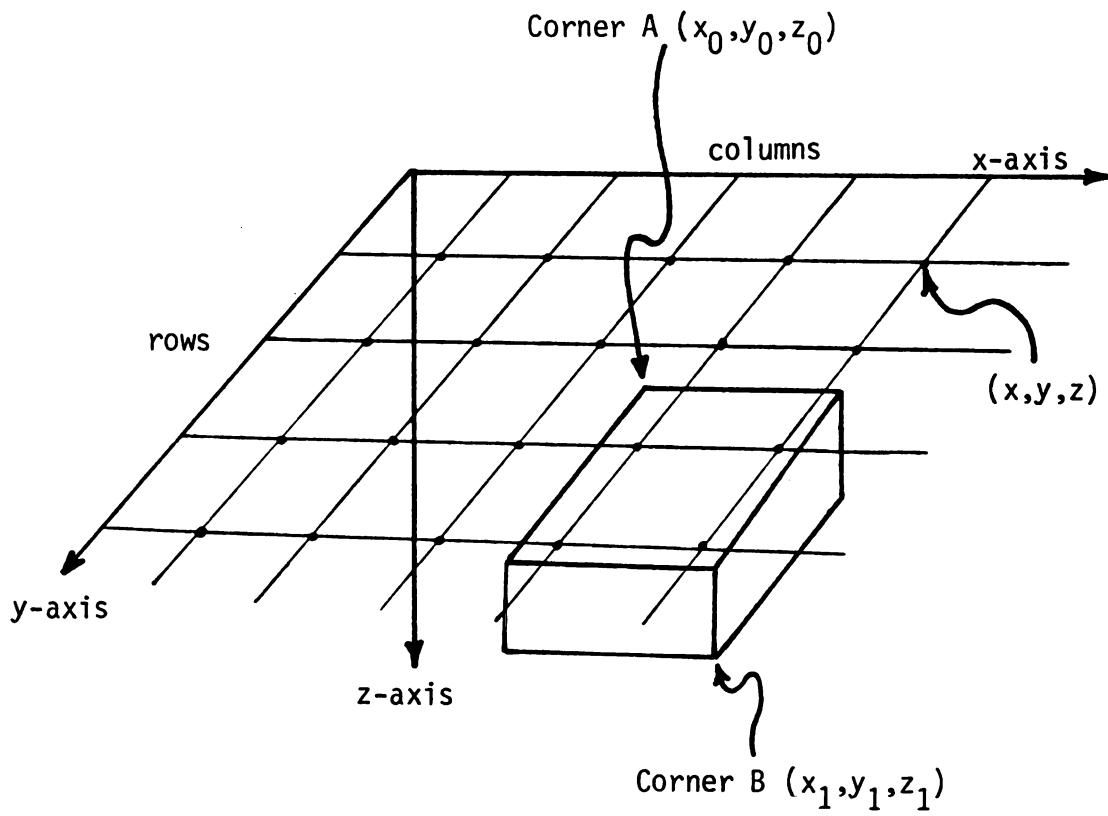


Figure 25. Coordinate system used in SHALOCI.

order to calculate the total magnetic field anomaly in the direction of the earth's field instead of the vertical magnetic field as SHALOCI does. The instructions for using SHIEK are exactly the same as those for SHALOCI but the user is reminded to remember that the output values are not the same.

SHALOCI allows the user to choose from a wide variety of output data types and formats, and also to control the number and size of prisms inputted. SHALOCI is also equipped with numerous error checking devices to aid the user in setting up and screening his data.

Preliminary Discussion

The coordinate system that SHALOCI uses is illustrated in Figure 25. The user determines the size and shape of the area for which magnetic values will be calculated by specifying the number of rows and columns the model is to contain. Values will be calculated at the points, marked by black dots in Figure 25, where row and column lines cross. This user-specified grid can be no larger than 40 by 40. The magnetic bodies over which this grid has been constructed, however, can extend for as far in any direction as the user desires. These buried bodies must be prisms whose sides are parallel to the x, y, and z axes, although individual prisms of this nature may be arranged so as to form a body of any shape or orientation the user desires. The user may input up to 50 prisms whose size, shape, and arrangement are controlled entirely by him. Each of these prisms is "echo" printed as it is read in so that the user can make sure that his input data is correct. This data consists of the coordinates of corner A, the coordinates of corner B as shown in Figure 25, and some information about

the magnetic properties of the prism. When modeling, please note that the x-axis points due north.

A Word About Units

In SHALOCI, all angles are read-in in degrees and printed out in radians. Magnetic field intensities are read-in in gammas and are printed out in the same units. Magnetic susceptibilities are read-in in cgs units multiplied by 10^5 (i.e., a susceptibility of 400×10^{-5} cgs units would be inputted as 400.0). The size dimensions of the grid and prisms are completely arbitrary as long as 1 unit on the x-axis = 1 unit on the y-axis = 1 unit on the z-axis. That is to say, 1 unit on the x-axis could be 1 mile, 1 kilometer, 10,000 feet, or any other distance that suits the user as long as the same distance is represented by 1 unit on the y and z axes.

Input for SHALOCI

The input data for SHALOCI can be split into three parts. The first part contains information about the model's location, and its size and shape. The second consists of information about the prisms over which the user's grid has been constructed. The last contains the control cards for the program's option package. All the data in these three parts must be decimal except where otherwise indicated. These non-decimal entries will be marked "ND."

Part 1: (1) card 1: In columns 1 to 5, type the declination of the earth's magnetic field in the area (0 to 359°) (see Figure 26); in columns 6 to 10, type the inclination of the earth's magnetic field in the model area (0 to 359°). Due to the restrictions of some of the program's equations, the

inclination can not be exactly 90° , 180° , or 270° ; in columns 11 to 15, type the latitude of the area (0 to 90°).

(2) card 2: Right-justified (i.e., as far to the right as possible) in columns 1 and 2, type the number of rows in the model, ND. This number should not exceed 40; right-justified in columns 3 and 4, type the number of columns in the model, ND. This number should not exceed 40; in columns 5 to 9, type the distance between the rows. The distance between the columns will be the same as the distance between the rows. (Note: if the number of rows or columns is set equal to 1, the output of the program becomes a 2-dimensional magnetic profile.)

Part 2: (1) card series 3: Leave columns 1 to 10 of this card blank. In columns 11 to 23, type the declination of the prism's remanent magnetic field (0 to 359°) (see Figure 27). In columns 24 to 36, type the inclination of the prism's remanent magnetic field (0 to 359°). In columns 37 to 49, type the strength (in gammas) of the prism's remanent magnetic field. If the user does not wish to consider the effects of remanent magnetism, leave columns 1 to 49 blank. In columns 50 to 62, type the magnetic susceptibility of the prism in cgs units times 10^5 (i.e., a susceptibility of .00010 cgs units would be typed as 10.0).

(2) card series 4: In columns 1 to 5, type the x-coordinate of corner A (see Figure 25). In columns 6 to 10, type the y-coordinate of corner A. In columns 11 to 15, type the z-coordinate of corner A. This coordinate can never be zero.

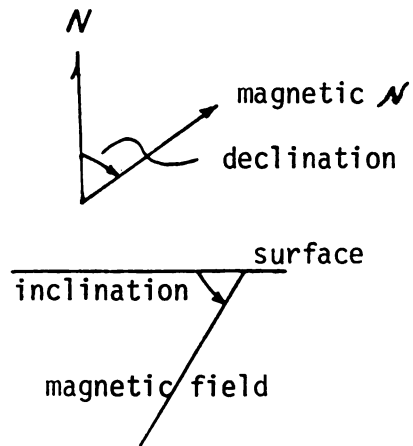


Figure 26. Magnetic declination and inclination

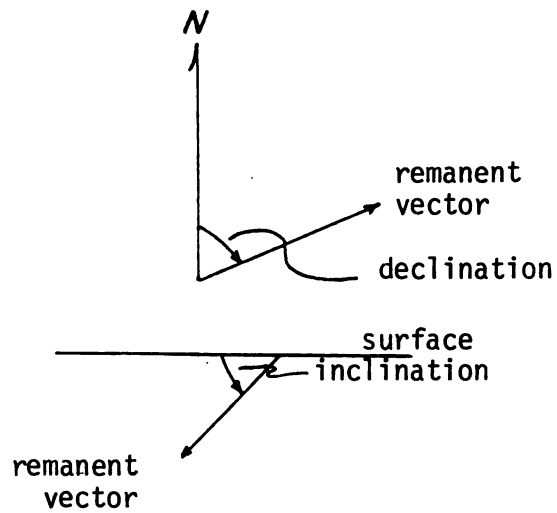
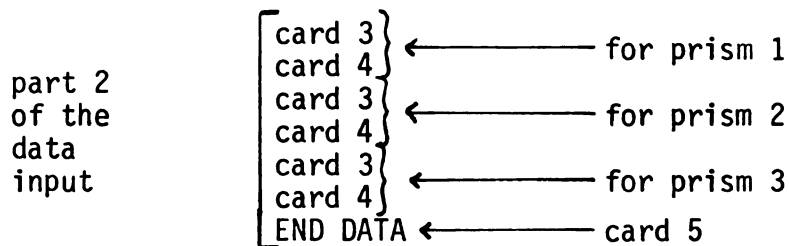


Figure 27. Remanent vector inclination and declination.

In columns 16 to 20, type the x-coordinate of corner B (see Figure 25). In columns 21 to 25, type the y-coordinate of corner B. In columns 26 to 30, type the z-coordinate of corner B. Corner A is always the corner closest to the origin on the top of the prism. Corner B is always the corner farthest from the origin on the bottom of the prism.

(3) card 5: The user continues to input the model's prisms, a card 3 and a card 4 for each, until the last prism has been inputted. Then in columns 1 to 8 of the very next card, the user should type END DATA. Thus, if the user's model contained 3 prisms, this part of the data deck would look like:



Part 3: (1) card 6: The option package control card. All entries are non-decimal. If the user wishes to input observed magnetic readings, he should type a 1 in column 1. Rows times columns values will then be read in and residuals (calculated - observed values) will be computed and printed out. The observed readings should be typed 8 per card, one every 10 columns. If the user does not want to input observed values, leave column 1 blank. If the user wishes to have a plot of SHALOCI's output in addition to the normal lineprinter output, he should type a 1 or a 2 in column 2. A 1 should be typed if the user wants a CALCOMP plot of the calculated magnetic values. A 2 should be typed if the user wants a CALCOMP plot

of the calculated magnetic values and the residuals explained above. Remember, a 2 cannot be typed unless a 1 was typed in column 1. If no plot is desired, the user should leave column 2 blank. If the user has requested a plot, the user now has a choice of two plot sizes. If the user wants the normal 15"-wide plot, the user should leave column 3 blank. If he wants the large 36"-wide plot, he should type a 1 in column 3. This next part of the option card allows the user to choose exactly what the magnetic values output by the program will mean. If column 4 is left blank, the vertical anomaly as calculated by the program will be output. If a 1 is typed in column 4, the total vertical intensity (the vertical component of the earth's field + the vertical anomaly) of the magnetic field over the model will be output. If a 2 is typed, the output will consist of the total vertical intensity of the magnetic field minus some arbitrary value specified by the user on card 9. Please note that this option has no impact on the residuals calculated if column 1 of this card is a 1. These residuals are always the calculated vertical magnetic values minus the observed values inputted by the user. The last option allows the user to request punched-card output. If no punched-card output is desired, leave column 5 blank. If a 1 is typed in column 5, the output will be punched on cards in a manner acceptable to the GEOSYS contouring package. If a 2 is typed in column 5, the output will be punched on cards in a manner acceptable to the SYMAP contouring package.

(2) card 7: On this card the user should type the name of

the magnetic model. The name can be composed of any combination of letters, numbers, and symbols the user desires.

(3) card series 8: If the user has typed a 1 in column 1 of card 6, the user must input the observed values here. The values should be entered 8 per card, observation 1 in columns 1 to 10, observation 2 in columns 11 to 20, and so on. The values should be typed in the following order: (1) starting in the upper left-hand corner of the grid, the user should proceed from left to right across the first row (see Figure 28), (2) the user should then proceed from left to right down the second row, entering the values there, and (3) this process should be repeated until all the rows have been done. The user should make sure that the observation grid matches the calculated model grid in all respects. Also, the last card of this series can have less than 8 entries.

(4) card 9: If a 2 is typed in column 4 of card 6, the arbitrary value that is to be subtracted from the total intensity should be typed in columns 1 to 15 of this card.

Deck Structure

The input deck for SHALOCI should be set up as follows:

Control Cards	Sequence card PNC Job card ATTACH, SHALOCI, SHALOCI. SHALOCI. multipunch 7-8-9
Data Cards	card 1 card 2 card 3 } ← prism 1 card 4 } : :

Data Cards (cont.)	<table border="0"> <tr> <td style="border-left: 1px solid black; padding-left: 5px;">card 3</td> <td rowspan="2" style="font-size: 2em; padding: 0 5px;">}</td> <td rowspan="2" style="vertical-align: middle;">← last prism</td> </tr> <tr> <td style="border-left: 1px solid black; padding-left: 5px;">card 4</td> </tr> <tr> <td style="border-left: 1px solid black; padding-left: 5px;">card 5</td> <td></td> <td></td> </tr> <tr> <td style="border-left: 1px solid black; padding-left: 5px;">card 6</td> <td></td> <td></td> </tr> <tr> <td style="border-left: 1px solid black; padding-left: 5px;">card 7</td> <td></td> <td></td> </tr> <tr> <td style="border-left: 1px solid black; padding-left: 5px;">card series 8 (if required)</td> <td></td> <td></td> </tr> <tr> <td style="border-left: 1px solid black; padding-left: 5px;">card 9 (if required)</td> <td></td> <td></td> </tr> <tr> <td style="border-left: 1px solid black; padding-left: 5px;">multipunch 6-7-8-9</td> <td></td> <td></td> </tr> </table>	card 3	}	← last prism	card 4	card 5			card 6			card 7			card series 8 (if required)			card 9 (if required)			multipunch 6-7-8-9		
card 3	}	← last prism																					
card 4																							
card 5																							
card 6																							
card 7																							
card series 8 (if required)																							
card 9 (if required)																							
multipunch 6-7-8-9																							

If the user has any questions or problems, he should contact David C. Shanabrook or Mark Fortuna.

Program SHIFT can be used to calculate either the upward and downward continuation of a potential field or its first and second derivatives. This type of information is very useful in determining the depth of the body that is producing a geophysical anomaly or in separating an anomaly from useless and confusing noise. The program, based on the work of Henderson (1960), allows the user a wide variety of selections in manipulating the initial input data and a good deal of control over the input data. The user is warned to read and completely understand the following theory section before using the program and trying to interpret its output.

Theory

The calculating equations for SHIFT are based on the solution of the Dirichlet problem for a half space:

$$P(-z) = \int_0^{\infty} \frac{(-z) \cdot P(r) \, dr}{(r^2 + z^2)^{1.5}}$$

where r is the radius of a circle around the central point, $-z$ is the point's height above the plane, and $P(0)$ is the potential field in the data plane. It can be shown that $P(r)$, the average value of the field on a circle of radius r , is given by:

$$\bar{P}(r) = \frac{1}{2\pi} \int_0^{2\pi} P(r, \psi) d\psi$$

More simply, however, $\bar{P}(r)$ can be approximated by the arithmetic average of the grid values intersected by a circle of radius r . For example, in Figure 29, $\bar{P}(r_1) = (6 + 7 + 8 + 12) \div 4 = 8.25$. Further simplifying by setting z equal to ka (i.e., making the height above the plane a multiple of the grid spacing), one obtains:

$$P(z) = P(ka) \doteq \sum_{i=0}^{10} P(r_i) C(r_i, k)$$

where $C(r_i, k)$ is a set of predetermined coefficients and k is an integer. It has been shown that this approximation is satisfactory when the radii, r_i , are $0, a, a\sqrt{2}, a\sqrt{5}, a\sqrt{8}, a\sqrt{13}, 5a, a\sqrt{50}, a\sqrt{136}, a\sqrt{274}$, and $25a$. This simplification is an outgrowth of the Lagrange interpolation formula for field fitting, which is also the basis for the derivative formulae used here.

Cautions

(1) For best results, the input data should be gridded at a spacing that is one-fourth the depth to the body believed to be causing the anomaly. The data should then be smoothed. If this is not done, any "spikes" or noise left in the data will render the program's calculations invalid and will cause errors in the results.

(2) If the output plane is downward continued into the causative body, the output results will "blow up."

(3) Since the program calculates along rings, linear features may begin to develop curvature when upwards or downwards continued 4 or more grid units.

(4) Severe interpretational problems can result when there are two or more bodies influencing the input data. If possible, the potential field of each body should be analysed separately. For example, if a profile of the input data looked like T, it would be necessary to split it into two parts, A and B, before it could be studied successfully (see Figure 30).

(5) Because of the way the program extends the data to avoid major edge effects, little faith should be put in the values near the edge of the output grid. Thus, the input grid should be centered over the anomaly of interest if possible. The pattern of extension is shown in Figure 31.

To sum up, then, the program first extends the data. Then it calculates the ring averages about each point. Next, it multiplies these averages by a series of weighting coefficients. Finally it sums the weighed averages at each point and outputs the results. If the user has any problems or questions, he should contact either David C. Shanabrook or Mark Fortuna.

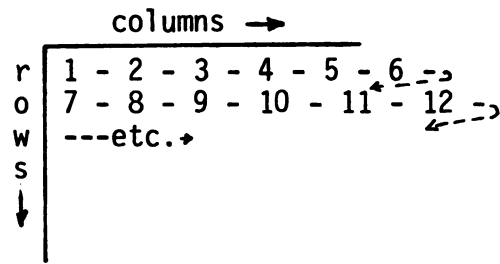


Figure 28. Order of data input for card series 8.

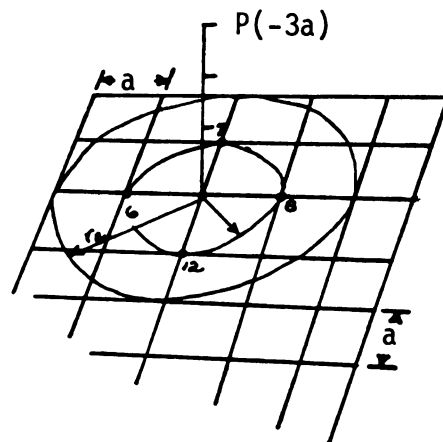


Figure 29. Example of ring-averaging.

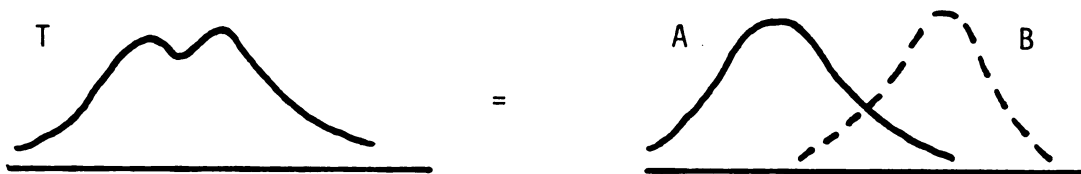


Figure 30. Anomaly separation for SHIFT.

25 by 25 filled with value A	A filled with edge values	B 25 by 25 filled with value B
filled with edge values	original data	filled with edge values
25 by 25 filled with value C	C filled with edge values	D 25 by 25 filled with value D

Figure 31. Data extension pattern of SHIFT.

APPENDIX B

Determining Remanent Vectors with SHALOCI

The magnetic anomaly associated with the Yellow Dog Plains Peridotite is a good example of how SHALOCI, or its sister program SHIEK, can be used in aiding magnetic interpretation. It was known from textural, geochemical, and paleomagnetic studies that the peridotite was of middle-Keweenawan, or Y, age (Morris, 1977), yet it had a positive total field magnetic anomaly instead of a negative one that one would expect (Figure 32). SHIEK was then used to solve this problem by removing the induced magnetic field from the observed data to reveal a large negative anomaly caused by the reversed natural remanent vector of Y-age (Figure 33). This was accomplished by:

(1) finding the peridotite's magnetic susceptibility by measuring the susceptibility of 30 2.54 cm diameter cores that were at least 12.70 cm long with a magnetic susceptibility bridge. The susceptibility was found to be $(415.0 \pm 16.9) \times 10^{-5}$ cgs units at the 95 percent confidence level.

(2) using this value and a crude model of the body (Figure 34) as input for SHIEK, the induced magnetic field's strength was determined for points on a grid with a 100-meter spacing above the body.

(3) the induced field's strength and a regional magnetic field of 59,000 gammas were then subtracted from the observed values (see Table 5). The residuals were then contoured (Figure 33) revealing a modest negative anomaly with a northwest-southeast grain and a shape

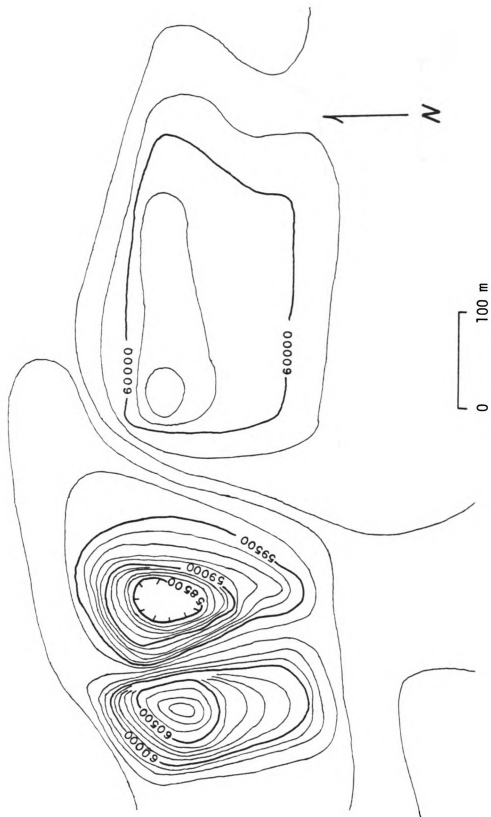


Figure 32. Observed total magnetic field values, Yellow Dog Plains Peridotite (c.i. = 100 gammas).

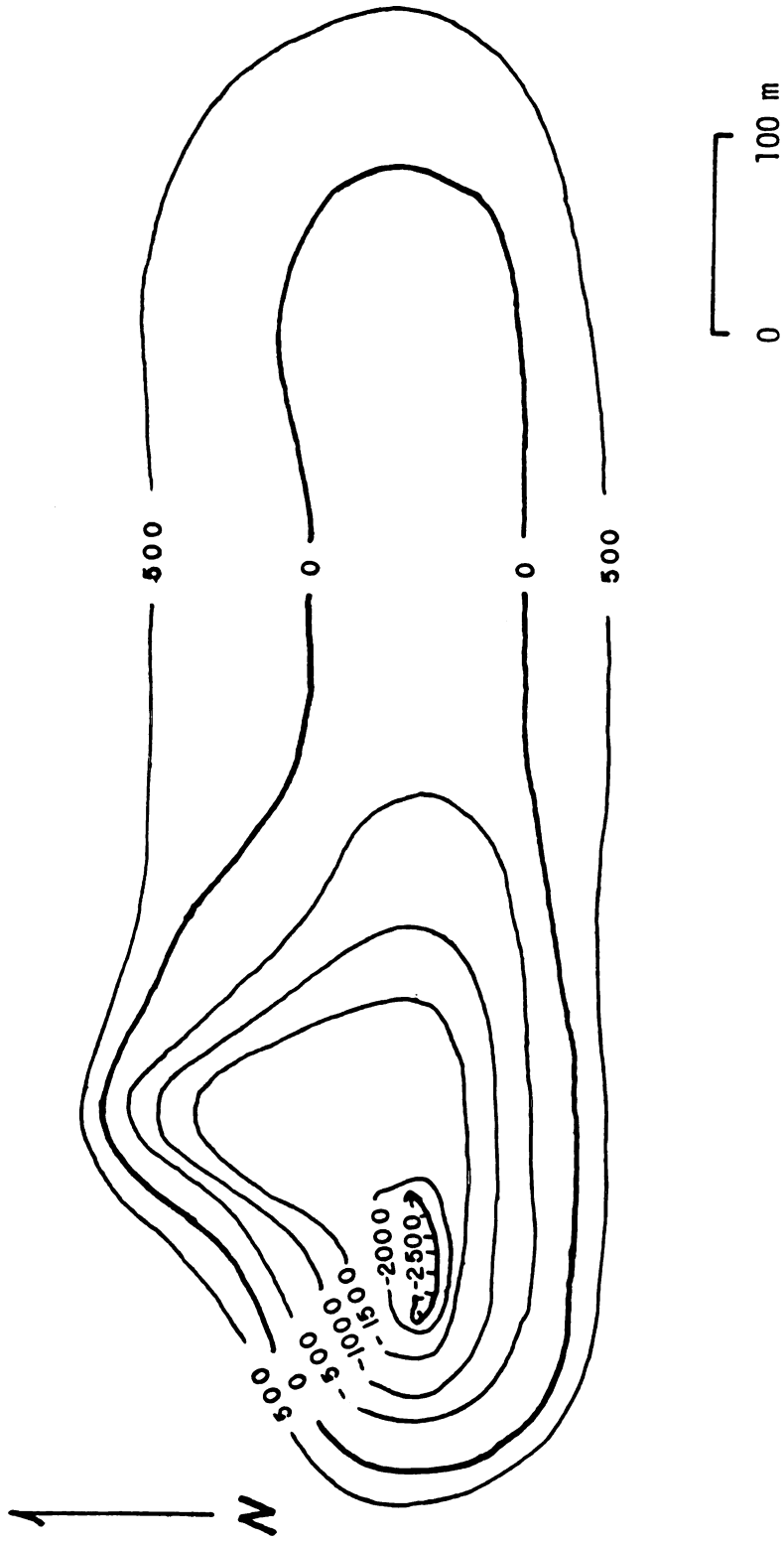


Figure 33. Natural remanent magnetic field, Yellow Dog Plains Peridotite (in gammas).

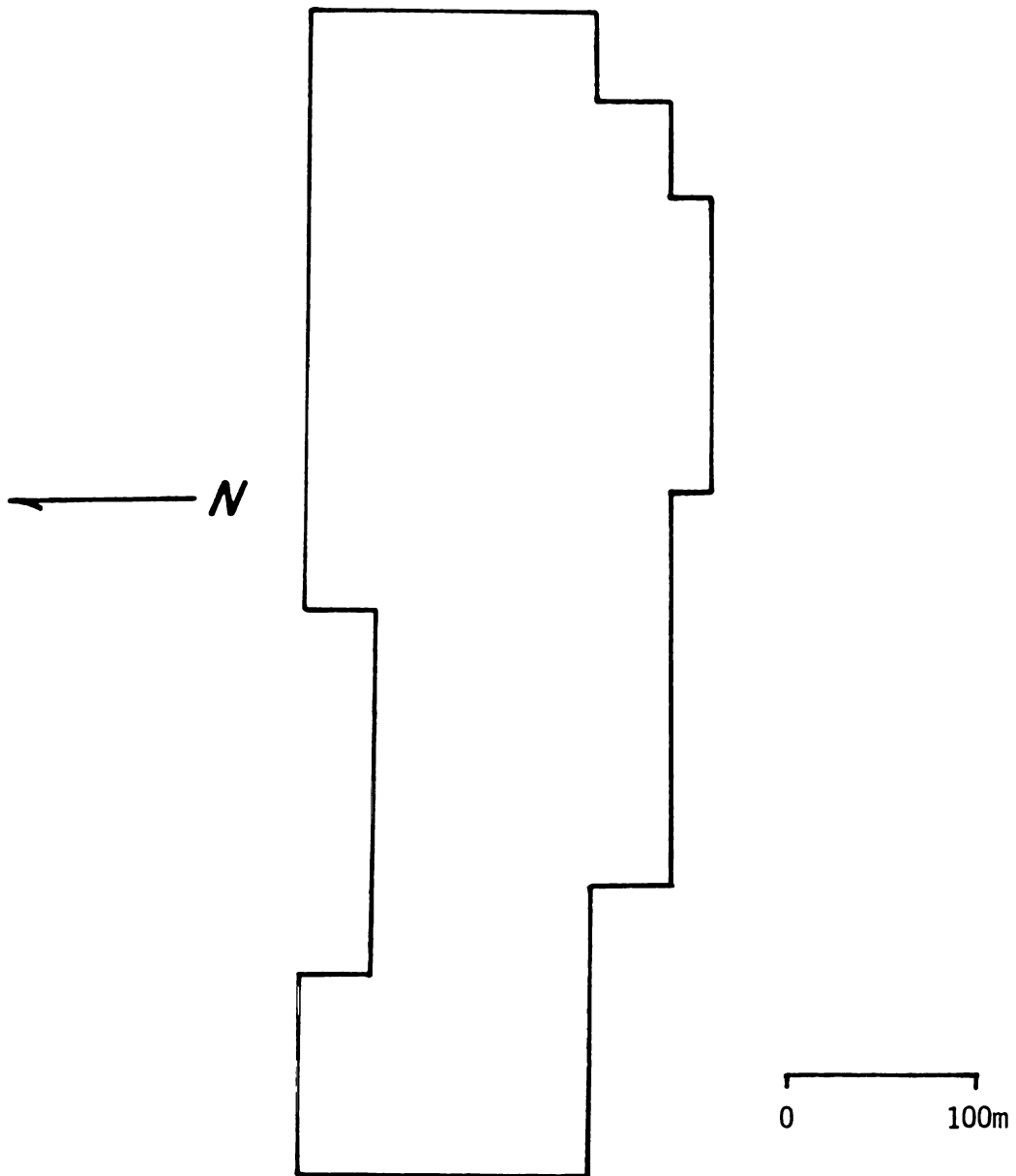


Figure 34. Model of the Yellow Dog Plains Peridotite.

Table 5. Yellow Dog Plains Peridotite - observed magnetic field values with the calculated induced field values (listed below observed value), and residuals.

distance from base line	EAST						
	400m	500m	600m	800m	1000m	1200m	
NORTH	600m	59751	59759	59739	59716	59717	59755
		-60	-86	-103	-127	-101	-42
	510m	59735	59709	59682	59668	59716	59752
		-95	-209	-201	-295	-240	-46
	390m	59646	60971	58165	60252	60126	59794
		-70	1129	824	934	1011	-29
	300m	59678	60199	59482	60020	60024	59786
	56	2814	2304	1498	1462	5	
210m	59704	59746	59778	59871	59849	59811	
	63	140	232	367	217	25	
90m	59820	59869	59789	59845	59872	59810	
	47	78	112	152	105	29	

residuals (amount above or below 59000 gammas):

	EAST					
	400m	500m	600m	800m	1000m	1200m
600m	811	845	842	843	828	797
510m	830	918	883	963	956	798
NORTH 390m	716	812	-1659	318	115	823
300m	622	-2615	-1822	-478	-438	781
210m	641	606	546	504	632	786
90m	773	791	677	693	767	781

that seems to indicate that the natural remanent vector points east-south-east and steeply upwards.

(4) various magnetic vectors were then fed into SHIEK in order to match the remanent magnetic field as closely as possible. After trying many different possibilities, a vector with a declination of 105 degrees and an inclination of -62 degrees was found to give the best fit. The unexplained residuals are tabulated in Table 6 and contoured in Figure 35. These residuals are never greater than 9 percent of the original magnetic value, and they do not seem to be associated with the magnetic body being modelled.

The remanent vector that was determined by this method varied only slightly from the vector obtained by paleomagnetic work on Keweenawan diabase dikes a few kilometers to the west, clearly establishing the peridotite's Keweenawan age. The remanent vectors' declination vary by 5.92 degrees while their inclinations vary by .17 degrees. The paleo-poles derived from these reversed remanent vectors are only separated by 4.6 degrees of latitude and 2.8 degrees of longitude which is well within the limits of error of the methods used. These results seem to indicate quite strongly that the computer-aided method for determining remanent vector orientation outlined above is a viable technique for magnetic bodies with strong remanent vectors that have not been badly altered by later metamorphism or other thermal events.

Table 6. Yellow Dog Plains Peridotite - calculated remanent magnetic field values and unexplained residuals.

distance from base line	EAST					
	400m	500m	600m	800m	1000m	1200m
600m	788	795	786	770	765	763
510m	836	868	836	950	960	787
NORTH 390m	780	818	-1707	312	117	835
300m	700	-2700	-1748	-410	-400	721
210m	690	631	533	545	600	707
90m	805	779	744	702	700	715

unexplained residuals (calculated value - residual from Table 5).

	EAST					
	400m	500m	600m	800m	1000m	1200m
600m	-23	-50	-56	-73	-63	-34
510m	6	-50	-47	-13	-4	-11
NORTH 390m	64	6	-48	-6	2	13
300m	78	-85	74	68	38	-60
210m	-49	-25	-13	41	-32	-79
90m	-32	-12	67	9	-67	-66

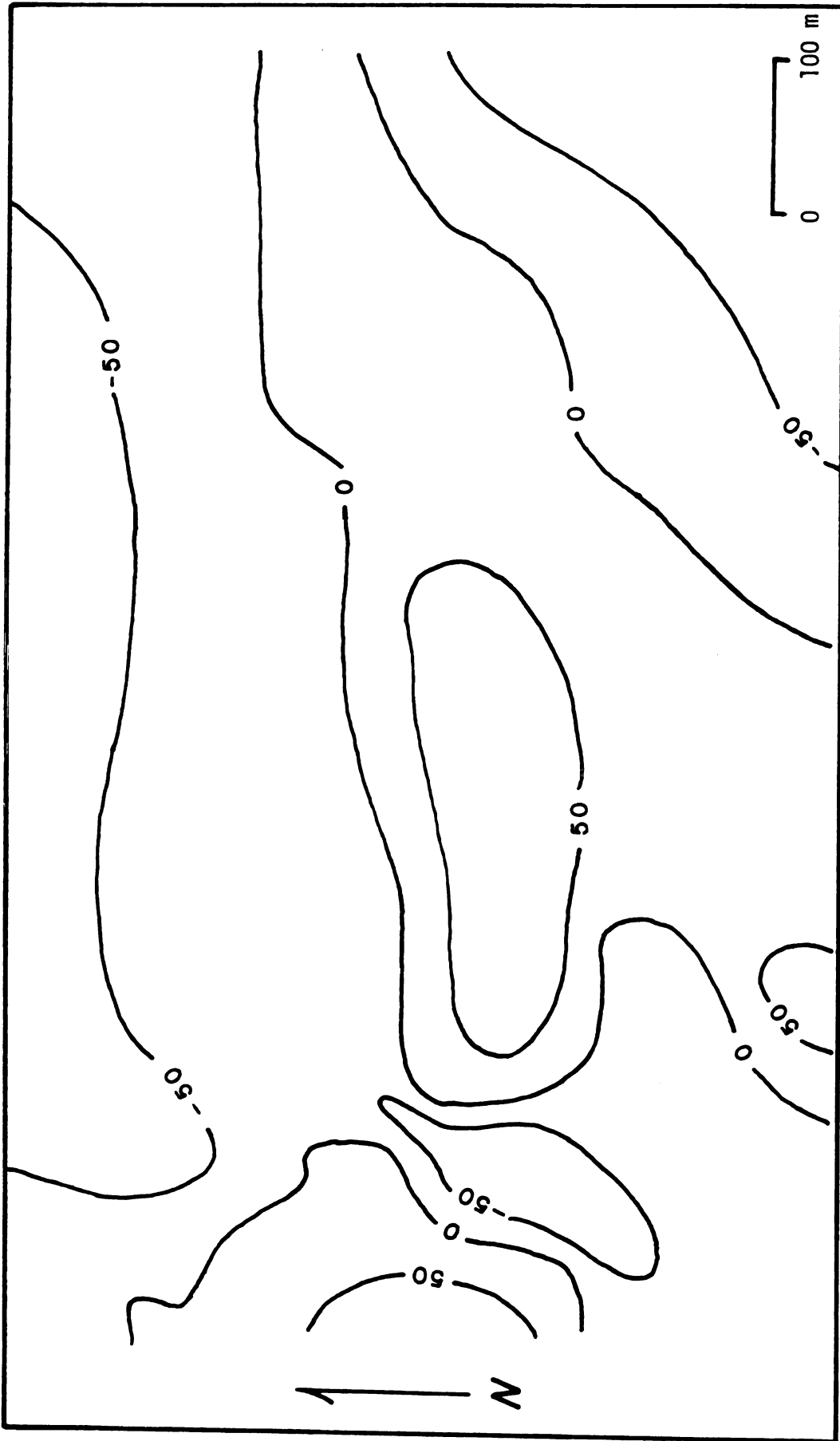


Figure 35. Residuals (model - observed) for the Yellow Dog Plains Peridotite (in gammas).

APPENDIX C

Paleomagnetic Data

Y-age Diabase

Original NRM vectors for Y-age diabase

<u>sample</u>	<u>declination</u>	<u>inclination</u>	<u>intensity (emu)</u>
12A2D	108.7	-63.7	.0751
12A2K	111.0	-66.0	.0793
12A2B	110.8	-67.5	.0656
12A2M	111.38	-66.59	.0731
12A2R	113.9	-62.8	.0632
12A2P	109.3	-64.5	.0839
12A2G	114.7	-63.3	.0599
12A2C	105.5	-62.7	.0863
12A2J	117.1	-63.3	.0893
12A2H	114.2	-62.3	.0902
12A1	193.3	- 0.1	.080
12A2T	114.4	-61.9	.0857
12A2S	113.1	-60.7	.0804
12A2E	111.7	-61.3	.0834
12A2I	114.8	-65.8	.0760
12A2N	112.1	-63.7	.0845
12A2F	93.4	-62.9	.0923
12A2O	106.3	-64.6	.0812
12A2Q	111.5	-60.7	.0886
12A2A	94.4	-63.4	.0662
12A2L	114.4	-61.4	.0679

Remanent directions after 100 oe AC field cleaning

12A2D	110.1	-62.3	.0759
12A2K	115.4	-63.7	.0820
12A2M	107.52	-64.59	.0752
12A2R	116.2	-62.1	.0656
12A2P	104.0	-62.7	.0831
12A2G	113.3	-63.0	.0596
12A2C	108.3	-62.1	.0882
12A2J	118.0	-61.0	.0904
12A2H	116.0	-61.0	.0921

Remanent directions after 150°C thermal cleaning

12A1	191.8	- 2.3	.0759
12A2T	112.7	-61.6	.0874
12A2S	109.9	-61.7	.0825
12A2E	110.8	-60.9	.0847
12A2I	112.4	-64.4	.0793
12A2N	111.7	-63.4	.0880
12A2F	108.9	-62.3	.0896
12A2O	110.7	-63.8	.0826
12A2Q	112.1	-60.3	.0909
12A2A	96.6	-53.8	.0541
12A2L	114.4	-62.0	.0694

X-age MetadiabaseOriginal NRM vectors for x-age metadiabase

<u>sample</u>	<u>declination</u>	<u>inclination</u>	<u>intensity (emu)</u>
9A22C	137.4	-27.2	.0344
9A22H	132.0	24.6	.0430
9A22D	161.2	36.2	.0172
9A22J	141.2	-47.7	.0045
9A22G	217.6	73.3	.0130
9A22I	145.8	-12.9	.0160
9A22A	121.8	-46.6	.0144
9A22E	146.9	55.3	.0297
9A22F	231.1	72.3	.0091
9A22B	195.6	80.4	.0161

Remanent directions after thermal cleaning

<u>sample</u>	<u>°C</u>	<u>declination</u>	<u>inclination</u>	<u>intensity (emu)</u>
9A22I	400	138.7	-14.9	.0036
9A22B	400	225.1	81.8	.0024
9A22B	475	12.5	13.1	.0018
9A22A	400	148.1	-52.4	.0028
9A22A	475	110.5	-16.5	.0008
9A22J	400	123.6	-38.2	.0016
9A22H	500	144.0	- 3.8	.0002
9A22D	500	184.8	-22.0	.0003
9A22G	500	112.4	2.0	.0001
9A22F	475	174.9	-13.7	.0019
9A22C	400	126.1	-34.5	.0042
9A22C	500	156.9	-28.1	.0003
9A22E	475	89.0	-17.4	.0020

BIBLIOGRAPHY

BIBLIOGRAPHY

- Beck, M. E., Jr., "Paleomagnetism of Keweenawan Intrusive Rocks, Minnesota", J. of Geophysical Research, v. 75, pp. 4985-4996, 1970.
- Berger, A. R., "Dynamic Analysis Using Dikes with Oblique Internal Foliations", Geological Society of America Bull., v. 82, pp. 781-786, 1971.
- Bhattacharyya, B. K., "Magnetic Anomalies due to Prism-Shaped Bodies with Arbitrary Polarization", Geophysics, v. 29, pp. 517-531, 1964.
- Bodwell, W., "Geologic Compilation and Nonferrous Metal Potential, Precambrian Section, Northern Michigan", M.S. thesis, Michigan Technological University, 1972.
- Books, K. G., "Magnetism of the Lowermost Keweenawan Lava Flows in the Lake Superior Area", U.S. Geological Survey Professional Paper 600-D, pp. D248-D254, 1968.
- Cannon, W. F., and J. E. Gair, "A Revision of Stratigraphic Nomenclatures for Middle Precambrian Rocks in Northern Michigan", Geological Society of America Bull., v. 81, pp. 2843-2846, 1970.
- Case, J. E. and J. E. Gair, "Aeromagnetic Map of Parts of Marquette, Dickinson, Baraga, Alger and Schoolcraft Counties, Michigan and its Geologic Interpretation", U.S. Geological Survey Geophysical Investigations Map GP 467, 1965.
- Chase, C. G. and T. H. Gilmer, "Precambrian Plate Tectonics: The Mid-continent Gravity High", Earth and Planetary Science Letters, v. 21, pp. 70-78, 1973.
- Goldich, S. S., A. O. Nier, H. Baadsgaard, J. H. Hoffman, and H. W. Krueger, "The Precambrian Geology and Geochronology of Minnesota", Minnesota Geological Survey Bulletin, v. 41, p. 193, 1961.
- Graham, J. W., "Changes of Ferromagnetic Minerals and Their Bearing on Magnetic Properties of Rocks", J. of Geophysical Research, v. 58, pp. 243-260, 1953.
- Henderson, R. G., "A Comprehensive System of Automatic Computation in Magnetic and Gravity Interpretation", Geophysics, v. 25, pp. 569-585, 1960.

- Irving, E. and J. C. McGlynn, "Proterozoic magnetostratigraphy and the tectonic evolution of Laurentia", Phil. Trans. R. Soc. London, v. A280, pp. 433-468, 1976.
- King, P. B., "The Tectonics of North America: A Discussion to Accompany the Tectonic Map of North America, Scale 1:5,000,000", U.S. Geological Survey Professional Paper 628, 1969.
- McElhinny, M. W., Palaeomagnetism and plate tectonics, Cambridge University Press, Cambridge, 1973.
- Morris, W. J., "Geochemistry and Origin of the Yellow Dog Plains Peridotite, Marquette County, Northern Michigan", M.S. thesis, Michigan State University, 1977.
- Palmer, H. C., "Paleomagnetism and correlation of some Middle Keweenaw rocks, Lake Superior", Canadian J. of Earth Sciences, v. 7, pp. 1410-1436, 1970.
- Robertson, W. A. and W. F. Fahrig, "The Great Logan Paleomagnetic Loop - The Polar Wandering Path from the Canadian Shield Rocks During the Neohelikian Era", Canadian J. of Earth Sciences, v. 8, pp. 1355-1372, 1971.
- Rudman, A. J. and R. F. Blakely, "Fortran Program for the Upward and Downward Continuation and Derivatives of Potential Fields", Department of Natural Resources Geological Survey Occasional Paper 10, State of Indiana, 1975.
- Tarling, D. H., Principles and Applications of Palaeomagnetism, Chapman and Hall, London, 1971.
- U.S. Geological Survey, "Aeromagnetic Map of the Keweenaw Bay Area, Michigan", Geophysical Investigations Map GP-608, 1967.
- Whitehill, D. E., "Automated Interpretation of Magnetic Anomalies Using the Vertical Prism Model", Geophysics, v. 38, pp. 1070-1087, 1973.
- Wittick, R. I., "GEOSYS: An Information System for the Description and Analysis of Spatial Data", Michigan State University Computer Institute for Social Science Research Technical Report 74-53, 1974.